NTIA Report TR-03-403

Measurements of Channel Transfer Functions and Capacity Calculations for a 16x16 BLAST Array over a Ground Plane

Peter B. Papazian
Yeh Lo
John J. Lemmon
Michael J. Gans

U.S. DEPARTMENT OF COMMERCE
Donald L. Evans, Secretary

Nancy J. Victory, Assistant Secretary
for Communications and Information

June 2003

CONTENTS

Page

FIGURES

Page

TABLES

Page

MEASUREMENTS OF CHANNEL TRANSFER FUNCTIONS AND CAPACITY CALCULATIONS FOR A 16X16 BLAST ARRAY OVER A GROUND PLANE

Peter B. Papazian, Yeh Lo, John J. Lemmon,* and Michael J. Gans**

Wideband channel transfer function measurements were made for a 16-element transmit and 16-element receive, multiple input, multiple output (MIMO) antenna array. The measurements were conducted using the National Institute of Standards and Technology (NIST) open area test site (OATS), allowing analytic calculations of the channel transfer functions. The H matrix for the BLAST array was then determined from measured data and the link capacity was calculated using information theory. The theoretical link capacity was then calculated and found to be 22.16 Bits/Hz/s for horizontally polarized antennas and 22.19 Bits/Hz/s for vertically polarized antennas. It was then found that the measured results agreed with the theoretical calculations with 5% error using horizontally polarized antennas and with <0.3% error for the vertically polarized case. The objective of this work was to verify that wideband measurements could be used to accurately measure H and predict the capacity of a MIMO channel.

Key words: BLAST; capacity; H matrix; impulse response; information theory; MIMO; radiowave propagation; transfer function

1. INTRODUCTION

It has been shown that the capacity of communications channels can be increased significantly by dividing the transmit power between multiple antenna elements and receiving with multiple antenna elements, when operating in a scattering environment [1,2]. This technique is called the "Bell Laboratories Layered Space-Time" (BLAST) communication technique in this report.

The narrowband channel capacity for a communications link with n_T transmitting antennas and n_R receiving antennas is:

$$C = \log_2 \left\{ \det \left[\mathbf{I} + \frac{\rho}{n_T} \mathbf{H}\mathbf{H}^{\dagger} \right] \right\} \text{ Bits/Hz/s,} \qquad (1)$$

where **H** is the normalized, narrowband complex transmission coefficient matrix from each transmitting antenna to each receiving antenna and ρ is an average signal-to-noise

* The authors are with the Institute for Telecommunication Sciences, National Telecommunications and Information Administration, U.S. Department of Commerce, Boulder, Colorado, 80305.
** The author is retired from Lucent Technologies, Holmdale, New Jersey.

ratio at the receiving antennas. The **H** matrix is normalized to signify an average power transmission over all combinations of transmitter antenna and receiver antenna of unity; i.e.,

$$\sum_{All\ j,k} \left| \mathbf{H}_{jk} \right|^2 = n_T n_R . \qquad (2)$$

$\mathbf{H}^{\dagger}$ is the Hermitian conjugate (transpose of the complex conjugate) of **H**. The normalization of Equation (2) is a result of the definition of ρ as the average signal-to-noise ratio at the receiving antennas when the total transmitter power is radiated from a single transmitting antenna. ρ is averaged over all combinations of transmitting and receiving antennas.

By measuring the transmission coefficient matrix, **H**, in a given environment, one can compute the channel capacity, *C*, of Equation (1). This can be computed for any assumed signal-to-noise level, ρ, of the communication link, which we term the *system* signal-to-noise level. The *measurement* signal-to-noise ratio, γ, is that which is achieved by the measurement equipment used to measure the transmission coefficient matrix, **H**. Clearly, one wishes to maintain a large γ in order to obtain accurate measurements of **H**. Once **H** is accurately measured, one can predict the link capacity for any system ρ , as mentioned above.

It is of interest to know how accurately **H** can be measured. This has never been done using a wideband measurement system in a known propagation environment. The National Institute of Standards and Technology (NIST) has an open area test site (OATS) in which one can accurately model an array transmission link. The site consists of a 60 m by 30 m metallic ground plane with mast sites separated by 30 m. Mounting plates at these sites are used to support the transmitting and receiving antenna arrays and allow access to underground tunnels to route cables below the ground plane. In this way, the cabling used for the two arrays is hidden from the propagation environment by the back planes of the antenna arrays and the ground plane. Simple half-wave dipoles are supported on the reflecting back planes to provide predictable patterns, with minimal mutual coupling due to the wavelength spacing of the array elements. A theoretical prediction of the channel capacity of such a communication link is given in [3,4] and in Section 8 and Section 9 of this report.

The remainder of this report is organized as follows: Section 2 describes the wideband transmitter and receiver and data acquisition system used for this experiment. Section 3 describes antenna arrays. Section 4 outlines the data processing procedure. Section 5 describes the psuedo noise coding used to identify transmitter elements. Section 6 discusses the system calibration methods. Section 7 describes the data collection procedures and the test data collected. Section 8 explains how the transmission link was modeled. Section 9 reports the results. Section 10 gives conclusions and Section 11 is the reference list.

2. TRANSMITTER AND RECEIVER OPERATION

Wideband measurements of the channel impulse response were made using a pseudo noise channel sounder. Figure 1 is a block diagram of the sounder's transmitter. Wideband signals are generated using a psuedo-noise (PN) sequence generator clocked by a 10-MHz rubidium frequency standard. The sequence generator (see Figure 2) is a self-controlled field programmable gate array (FPGA) and uses a maximal length shift register code of length 511 chips clocked at 10 mega-chips per second. Using the FPGA, the 16 outputs from the code generator are successively delayed by 32 chips (3.2 micro-seconds) relative to the previous output. These delayed codes are orthogonal. Thus the impulse response of each transmitter is able to avoid interference with all other transmitters provided the propagation delay spread is less than 32 chips (3.2 microseconds or 0.9 km). In this way, the sequences can be transmitted simultaneously and continuously using the rubidium clock reference signal, and the transfer matrix can be measured at the receiver.

Figure 3 shows a picture of the up-conversion and RF portions for 4 channels of the transmitter. The PN sequences are level shifted by a wideband limiter to create ±1 outputs that are then low-pass filtered (LPF) for pulse shaping. The 10-MHz clock also synchronizes a 2.3-GHz local oscillator which is split 16 ways and used to feed the 16 upconverter mixers that provide a 20-MHz bandwidth RF signal, to each of the power amplifiers. The power amplifiers operate at +22 dBm. The output RF filters eliminate unwanted sidebands in the simultaneous radiation from the 16 antenna elements.

A 4-channel receiver is time-shared between 4 groups of 4 receiving antenna elements to achieve the measurement capability of a 16-element receiver. The switching between each of the 4 antenna groups is accomplished in 80 nanoseconds using a multiplexer (MUX). For this experiment the MUX was operated manually at 10-second intervals. Since the antennas and environment were stationary, automatic fast switching was not necessary. For each group of 4 antenna elements, a burst of impulse data was collected.

Figure 4 shows a block diagram of the 4-channel receiver. The signals received by the antenna array are first filtered with preselection filters (Figure 5) to eliminate out-of-band interference before amplification by low noise amplifiers. A 2.14-GHz local oscillator, synchronized to the same rubidium clock, is used to down-convert the signal to the first IF of 160 MHz. The signal is then filtered to remove unwanted sidebands and amplified. A programmable analog gain control (AGC) amplifier is then inserted to provide 70 dB dynamic range with constant output levels for the digitizers. The AGC control loop averages output power over one millisecond and the AGC level control data is output to the data recording equipment. The IF is then downconverted with a 150-MHz local oscillator, again synchronized by the rubidium clock, to a signal centered at 10 MHz. The second local oscillator frequency is chosen to maintain an output signal that is periodic at the sequence length duration (51.1 μsec). The 4-channel receiver outputs analog data to a VME bus 8-bit digitizer, sampling at 40 mega-samples per second (MS/s). Since the maximum frequency of the second IF only extends to 20-MHz, the sampling rate meets the Nyquist requirement.

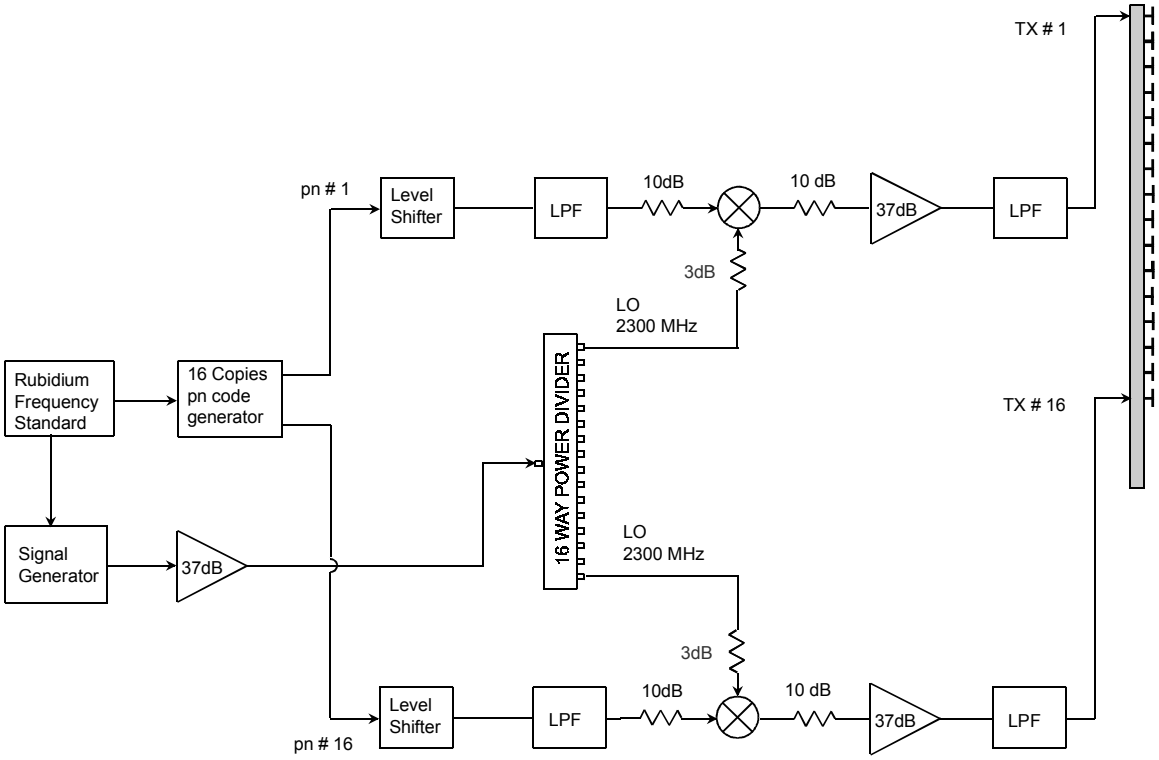

Figure 1. 16-channel wideband sounder transmitter.

Figure 2. 16-channel FPGA P/N code generator at transmitter.

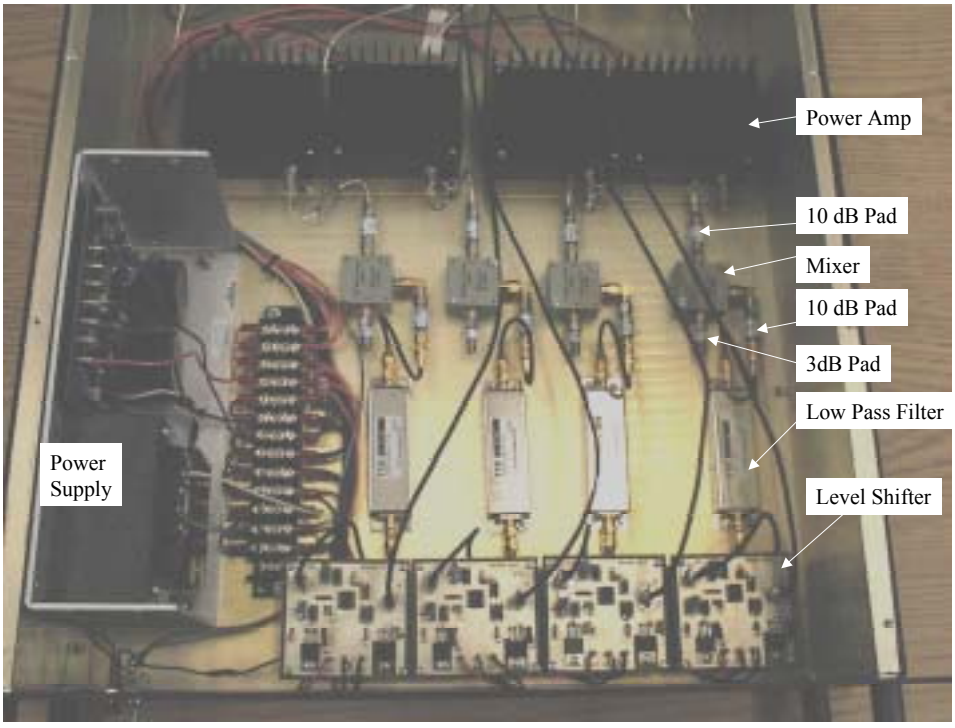

Figure 3. 4 RF channels of 16-channel transmitter array.

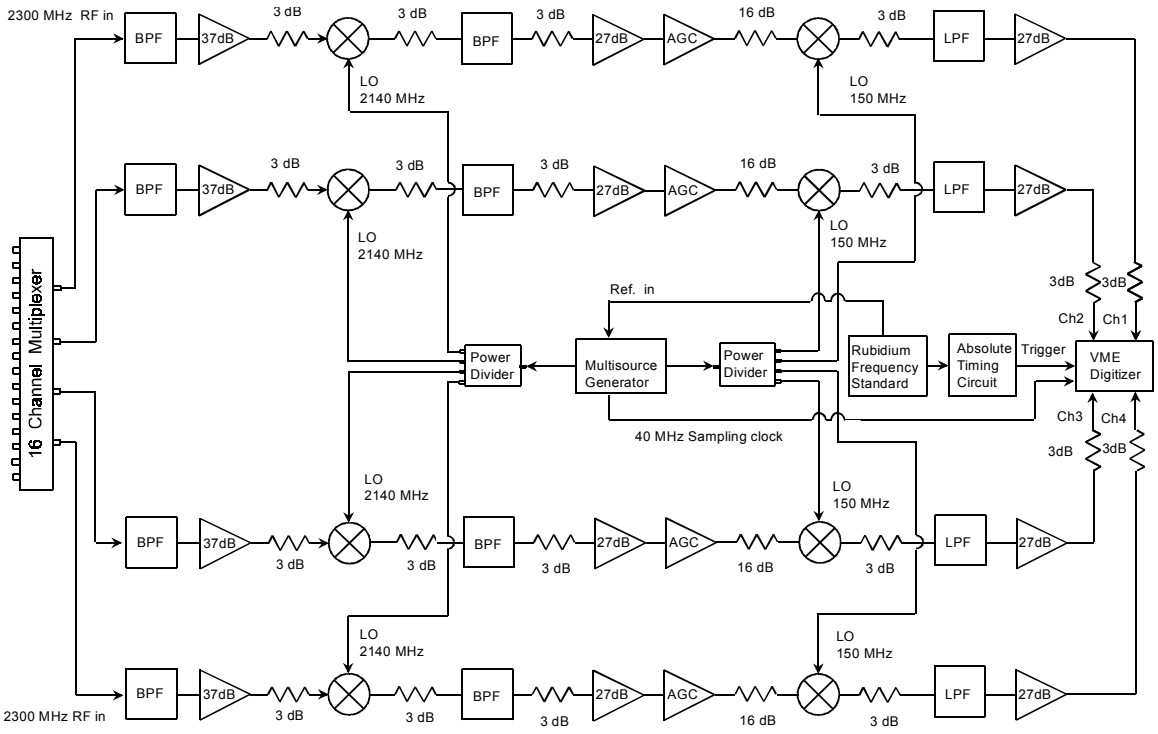

Figure 4. Block diagram of 4-channel receiver.

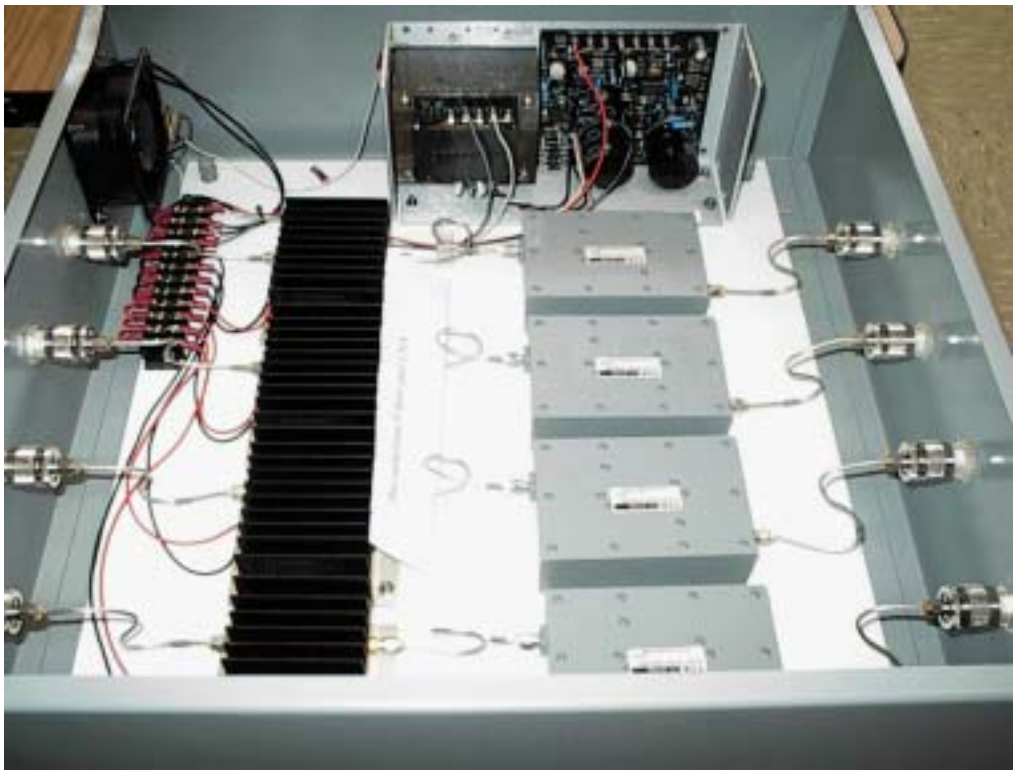

Figure 5. Preselector filters and low noise amplifiers of 4-channel receiver.

The VME digitizer has its own dedicated 2-Gbyte hard drive to which the data is streamed at a rate of 2 Mbytes per second. The FPGA timing circuit at the receiver controls the data sampling and recording. It is configured to record a burst of 128 impulses, 51.1 μs long with 3 milliseconds between impulses (2044 8-bit samples per receive channel per impulse). The receiver then waits 10 seconds while the antenna multiplex switch is set to receive the next set of 4 antennas. Thus a complete set of data for the 16 transmit elements by 16 receive elements is about 4.1 Mbytes plus 800 bytes of AGC data and other overhead information in file headers. A block diagram of the data acquisition and storage equipment is shown in Figure 6.

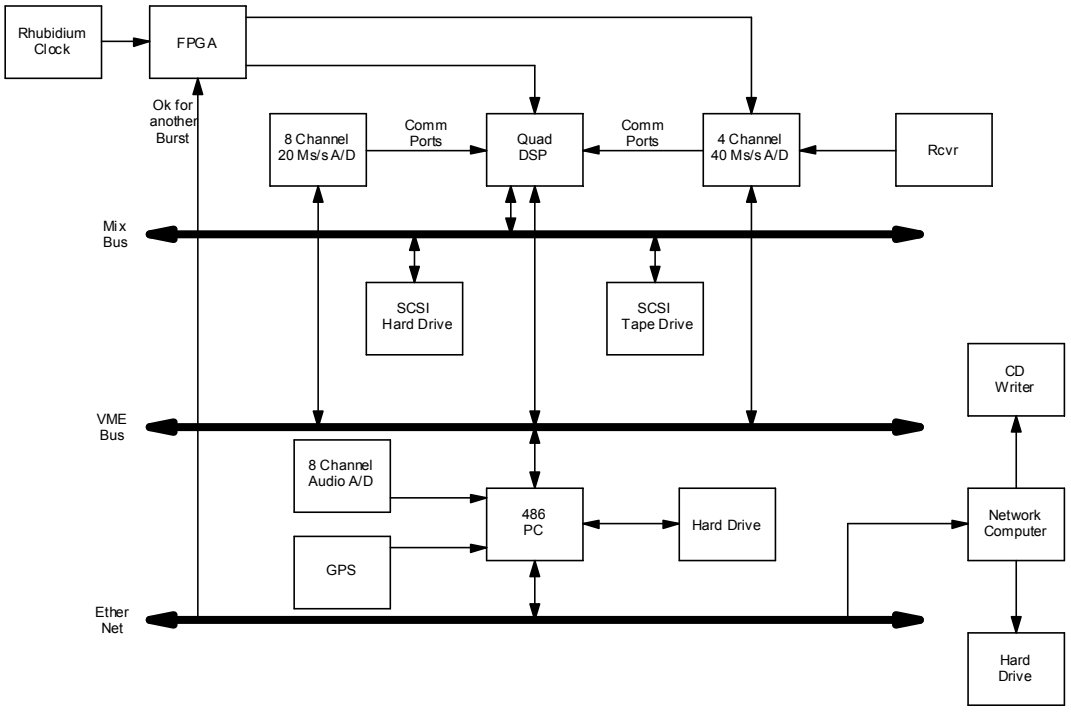

Figure 6. Block diagram of data acquisition system.

Raw data can be sent to the network computer for further processing and archived on CD ROMs. The raw data is a collection of the digital samples of all the received waveforms. These digital samples are then processed in the PC or in the network computer to obtain the impulse response representation of each transmission matrix element corresponding to a given transmitting antenna element and a given receiving antenna element.

3. ANTENNAS AND GROUND PLANE

The antenna elements are half-wave dipoles mounted one-quarter wavelength above a reflecting back plane. The back plane allows the dipole feed cabling to have negligible interaction with the propagation between the transmitting and receiving arrays. The dipole elements are spaced one wavelength apart (0.13m) along a vertical from 17.5 wavelengths above the ground plane to 32.5 wavelengths at both the transmitter and receiver. The aluminum back planes are 4 wavelengths wide, extending from the ground plane to a height of 34.5 wavelengths. The distance from the transmitting array to the receiving array is 231.71 wavelengths (30.2m), and the arrays are centered on the 60 m by 30.5 m ground plane. The arrays and ground plane are shown in Figure 7 and Figure 8.

Figure 7. Antenna arrays on ground plane, the closer array is the receiving antenna. The antenna elements are shown in Figure 8.

Figure 8. Dipole antenna elements in vertical array.

The ground plane is terminated along its edges with triangular serrations to minimize edge reflections, so that the propagation is well approximated by dipoles over an infinite ground plane. This feature allows for a simple analytic model of the communications channel described in Section 8. The receiving antenna cables are fed under the ground plane and through a tunnel approximately 8 m long to the receiving and data recording equipment. The transmitter equipment was shielded from the experiment by the transmit array backing plate. The cables connecting the transmitter to the antenna elements were approximately 5 m long. Receiver equipment is located in a climate-controlled room at the end of the access tunnel under the receive array and ground plane. Coupling between cables was measured to be less than –100 dB. The mutual coupling between antenna elements was measured using a network analyzer over the 20-MHz band centered at 2.3

GHz. These results are discussed in section 7.5 and reported in detail in Appendix B. It was concluded that the mutual coupling between antenna elements had a negligible effect on the **H** matrix magnitude measurements. The antenna patterns were measured for all the antenna elements over 4λ backing plates. The backing plates increased the forward gain of the elements. The antenna impedance match was better than 10 dB return loss over the band. The cross-polarization discrimination was better than 30 dB in most directions. The antenna patterns were matched over all the elements to within .1 dB at boresight and 1 dB in most directions. More details on antenna calibration are given in sections 7.5 and 7.6.

4. DATA PROCESSING

Post acquisition processing of the digitized IF signal provides impulse response data for all the receiving antenna elements. This impulse data is then processed to yield the **H** matrix required by Equation 1 for the capacity calculation. There are several steps in the processing that include down conversion, correlation, transmitter receiver channel identification, and calibration which are performed prior to the calculation of the **H** matrix.

The first stage of the processing is to down convert the real IF signal to complex baseband; this is done in the time domain. These results are then transformed into the frequency domain using a discrete Fourier transform (DFT) and then low pass filtered to remove unwanted side lobes. A copy of the transmitted PN code is also transformed to the frequency domain using a DFT and then the data and the PN code are convolved at baseband by multiplying the Fourier coefficients of each transform. The result is a band limited system response for each antenna element. This data can then be translated back to the time domain using an inverse DFT. Since each transmit antenna broadcasts a delayed version of the same psuedo noise sequence, each transmitter can be identified by its delayed impulse response. These signals are separated in time, zero padded and transformed back to the frequency domain where a 16x16 calibration matrix can be convolved with each matrix element corresponding to the 256 channel transfer functions.

After multiplication by the calibration constants for each transmitter receiver pair, the calibrated transmission matrix is normalized to produce the **H** matrix. The psuedo noise sequence transmitted is defined in Section 5 and the calibration matrix is described in Section 6.

5. CHARACTERISTICS OF THE PN SEQUENCE

The PN sequence is stored in ROM memory on the FPGA chip. The stored sequence is equivalent to the output of a shift register with 9 delays and 2 modulo 2 additions connected for a maximal length sequence at taps 4 and 9, as shown in Figure 9.

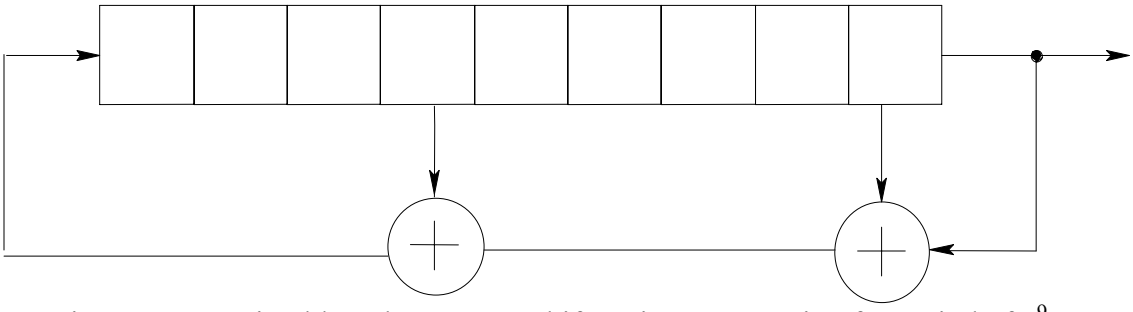

Figure 9. Maximal length sequence shift register connection for period of 2^9-1 (511) chips.

6. SYSTEM CALIBRATION

A series of wideband system calibration measurements were made without antennas in preparation for BLAST testing. The purpose of these calibrations was to determine relative amplitude and phase calibration between receiver channels. Additionally, these data can be used to determine the system response of each measurement channel in order to deconvolve the effects of the measurement system. The calibrations were completed using two system configurations that produced two sets of raw calibration data.

The first configuration is called TxCal. This configuration utilized all transmitter channels fed through the transmitter cables, arrayed as they were to be used during the testing, into an N-Type coupler and then connected to the appropriate receiver cabling and through the MUX to the receiver and digitizers. The output power for each transmitter is constant but can be varied in 10-dB steps using a set of precision attenuators. Each transmitter power level was measured at the coupler and stored. The power level was then varied over a 70-dB range to check the linearity of the AGC, receiver dynamic range and sensitivity. In this way each receiver channel can be calibrated for transmitter power levels as referenced to the receiver antenna terminal. The data for this calibration is stored in 4 data files consisting of 7 bursts of data. Each burst has 128 impulses for 4 channels at one power level.

The second configuration is called RxCal. Here one transmitter channel is utilized to provide identical signals to all 16-receiver channels using the antenna cabling and all the hardware except the antennas used for the BLAST tests. Using this data the system calibration can be described using the following equations.

The system response calibration matrix c_{ij} is

$$c_{ij} = T_i R_j \ , \tag{3}$$

where T_i is the transfer function of the i^{th} transmitter and R_j is the transfer function of the j^{th} receiver. The TxCal configuration provides measured values of c_{ii} , $i=1,...,16$. The RxCal configuration provides measured values of c_{1j} , $j=1,....,16$. The remaining elements of c_{ij} can be determined from the measurements by writing c_{ij} as

$$c_{ij} = T_i R_j = T_i R_j \frac{T_1}{T_1}\frac{R_i}{R_i} = T_i R_i \frac{T_1 R_j}{T_1 R_i} = \frac{c_{ii} c_{1j}}{c_{1i}} . \tag{4}$$

7. DATA COLLECTION FORMATS AND PROCEDURES

This section describes the data collection procedures for the BLAST tests. Wideband data was collected using the 16-channel pseudo-noise transmitter, 4-channel wideband receiver, and 4-channel A/D section configured for burst mode acquisition. The burst mode combined with a 16-channel multiplexer (MUX) enabled the 16 receive antenna signals to be recorded as multiple data bursts in a single or multiple data files. Each burst of data consists of 128 impulses per channel with 2044 IF samples per channel per impulse sampled at 25-ns intervals (40-MHz rate). The delay between impulses is set to 3 ms and the delay between bursts to 10s. Channel data were stored using multiple data file configurations for different wideband tests and these configurations are described in the following sub-sections.

7.1 16x16 BLAST Test

This was a fundamental test, as it was accomplished with simultaneous transmissions from all transmitters. To record this data on the 4-channel receiver it required the 16-channel MUX. The MUX was manually switched 4 times between data bursts allowing 16 receive antenna signals to be recorded in one data file. This file contained 4 bursts of data. If all transmitters were operational this resulted in a 16x16 data set. Each receiver antenna element senses the 16 signals that were transmitted simultaneously. The integer A/D values along with header and AGC data corresponding to the received voltage v_j for each receive antenna element, $j=1,2....\ 16$, are stored in one file. The data structure can be summarized using the burst # and channel number as follows:

Burst 1 Ch1 = v_1,
Burst 1 Ch2 = v_2,
Burst 1 Ch3 = v_3,
Burst 1 Ch4 = v_4,
Burst 2 Ch1 = v_5,

Burst 2 Ch2 = v_6,

-
-

Burst 4 Ch4 = v_{16}.

7.2 1x16 BLAST Test

These tests used one transmitter channel and 16 receive channels (1x16) 16 times to collect the 256-element channel matrix data. The objective was to increase the signal-to-correlation noise level of the measured channel impulse response. This should have decreased the correlation noise level caused by transmitting 16 codes simultaneously. Since an increase in the signal to correlation noise level was not observed, this indicated that the psuedo noise generator was not the limiting factor. It is assumed that noise and distortion generated by analog components like filters in transmitter and receiving circuitry limited the signal to correlation noise level.

By manually switching the MUX between data bursts, 16 receive antenna signals were recorded in one data file. Because only one transmitter at a time was operational, this resulted in a 1x16 BLAST data set. By repeating the procedure 16 times, a 16x16 BLAST data set was recorded. When a 1x16 data set was being recorded all unused transmitters and transmitter antenna elements were terminated into 50 Ω loads. The recorded integer A/D values correspond to the receive antenna element voltages $v_{i,j}$, where i is the transmitter number and j is the index for the receive antenna element number. The data structure can be summarized using the file #, burst #, and channel number as follows:

File1 (Tx1)	**File2 (Tx2)**	**File3 (Tx3)……...File 16 (Tx16)**
Burst 1 Ch1 = $v_{1,1}$	Burst 1 Ch1 = $v_{2,1}$	Burst 1 Ch1 = $v_{16,1}$
Burst 1 Ch2 = $v_{1,2}$	Burst 1 Ch2 = $v_{2,2}$	
Burst 1 Ch3 = $v_{1,3}$		
Burst 1 Ch4 = $v_{1,4}$		
Burst 2 Ch1 = $v_{1,5}$		
Burst 2 Ch2 = $v_{1,6}$		
•		
•		
•		
Burst 4 Ch4 ($v_{1,16}$)	Burst 4 Ch4 = $v_{2,16}$	Burst 4 Ch4 = $v_{16,16}$

7.3 Keyhole Test

The objective of these tests was to determine the measurement signal to noise level, γ. These tests were made using the 16-channel transmitter and a power splitter at the receiver. $v_{1,1}$ was split 16 ways and fed into the MUX to all 16-receiver channels. Unused receiving antennas were terminated into 50 Ω loads. This data was not analyzed because

it was clear from the received power levels that the measurement signal to noise level was in excess of 30 dB. Data for the keyhole test were stored in one data file containing 4 bursts of data as in the 16x16 BLAST tests.

7.4 CW Tests

CW tests utilized a signal generator tuned to 2300 MHz at the transmitter. The signal source was used to feed single transmitting antenna elements. Power at the transmit antenna terminals varied from –11.8 to –10 dBm (see Appendix D). The received signal strengths were measured using a spectrum analyzer and corrected for receiver cable loss to yield the received signal power at the antenna terminals. These data were collected for comparison with the wideband results.

7.5 Antenna Coupling Tests

Antenna coupling was measured using a vector network analyzer (VNA). These tests were performed on the receiving antenna array in-situ over the ground plane. All receiver cables were in place and configured as in the BLAST testing (see Figure 7). The VNA was calibrated for 2-port operation with the measurement plane situated at the end of the antenna cables. After calibration, a through measurement was recorded using port 1 and port 2 cables only. The through VNA calibration is labeled in the data log (Appendix A) as Cal. For coupling tests the stimulus cable was hooked to port 1 on the VNA and the receiver cable was hooked to port 2. Data is stored in HP CITI format on disks, as summarized in Tables A1 and A2. Tables A1 and A2 also give a summary S_{12} or S_{21} in dB at 2300 MHz.

From the tables in Appendix A, we see that $S_{12} = S_{21}$, and antenna coupling between adjacent antenna elements is ≤ -20 dB for horizontal polarization and ≤ -30 dB for vertical polarization. Coupling then decreases with increased element separation. The phase and amplitude data are archived in case more detailed modeling of the H matrix is required in the future. For our purposes the coupling was sufficiently small to allow the magnitude of **H** to be measured without including the coupling terms in the analysis. An analytical coupling analysis also indicated that antenna element coupling could be ignored.[*]

7.6 Antenna Element Calibration

35 dipole antenna elements were manufactured using designs for a 1.92-GHz dipole antenna and then scaled to 2.3 GHz. Tests were performed in an anechoic chamber to confirm the performance of the scaled antenna elements. The tests were made using a calibrated standard gain horn as transmitter. The antenna under test (AUT) was mounted

[*] M.J. Gans, Personal Communication, June 2002.

on a 4λ square ground plane and the center of rotation of the test fixture was aligned to the ground plane. A prototype antenna numbered L01 was first tested in the anechoic chamber by making co-polarized and cross-polarized E and H scans over a 100-MHz frequency range. This data was used to confirm that the frequency scaling worked and that the cross polarization discrimination met the design specifications of -40 dBC. Co-polarized and cross-polarized patterns for L01 at 2300 MHz are shown in Figures 10 and 11. After it was confirmed that the antenna met specifications, 34 additional elements were made with sequential serial numbers. These elements were then tested, but this time only at the center frequency of 2300 MHz. These tests were used to determine if the machining process was uniform and that the antennas had similar gain and phase responses. It was found that all 35 elements had a gain variation of not more than 0.5 dB and phase variability of about ± 4° at bore sight at 2300 MHz. This allowed all transmitting and receiving antennas to be treated as identical elements in the analysis sections. These test data are summarized in Appendix B, Table B-1 and Table B-2. Raw antenna scan data are stored in TAR format. Since all elements were almost identical, numbers L1-L16 were chosen for the receiver antenna array and numbers L17-L32 were used for the transmitting antenna array (see Figures 7 and 8).

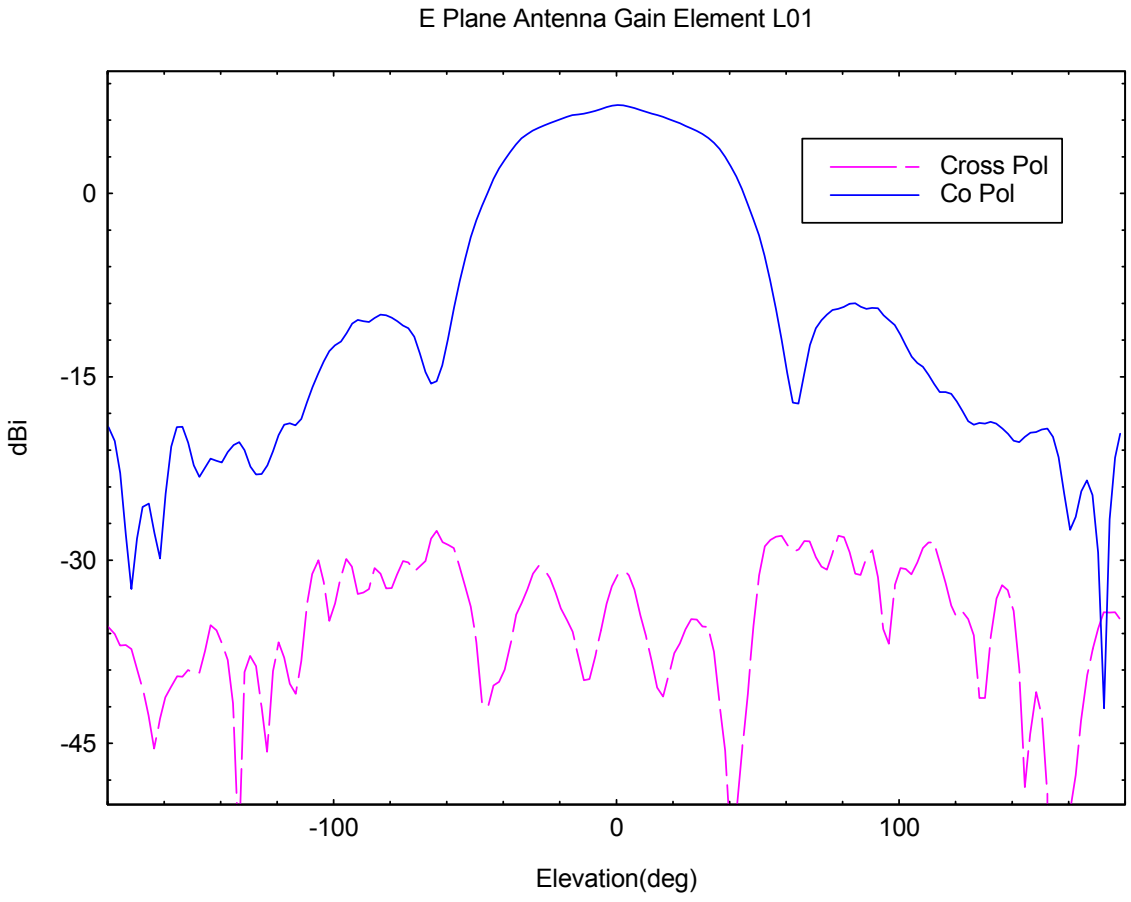

Figure 10. E-plane co-polarized and cross-polarized antenna patterns for element L01.

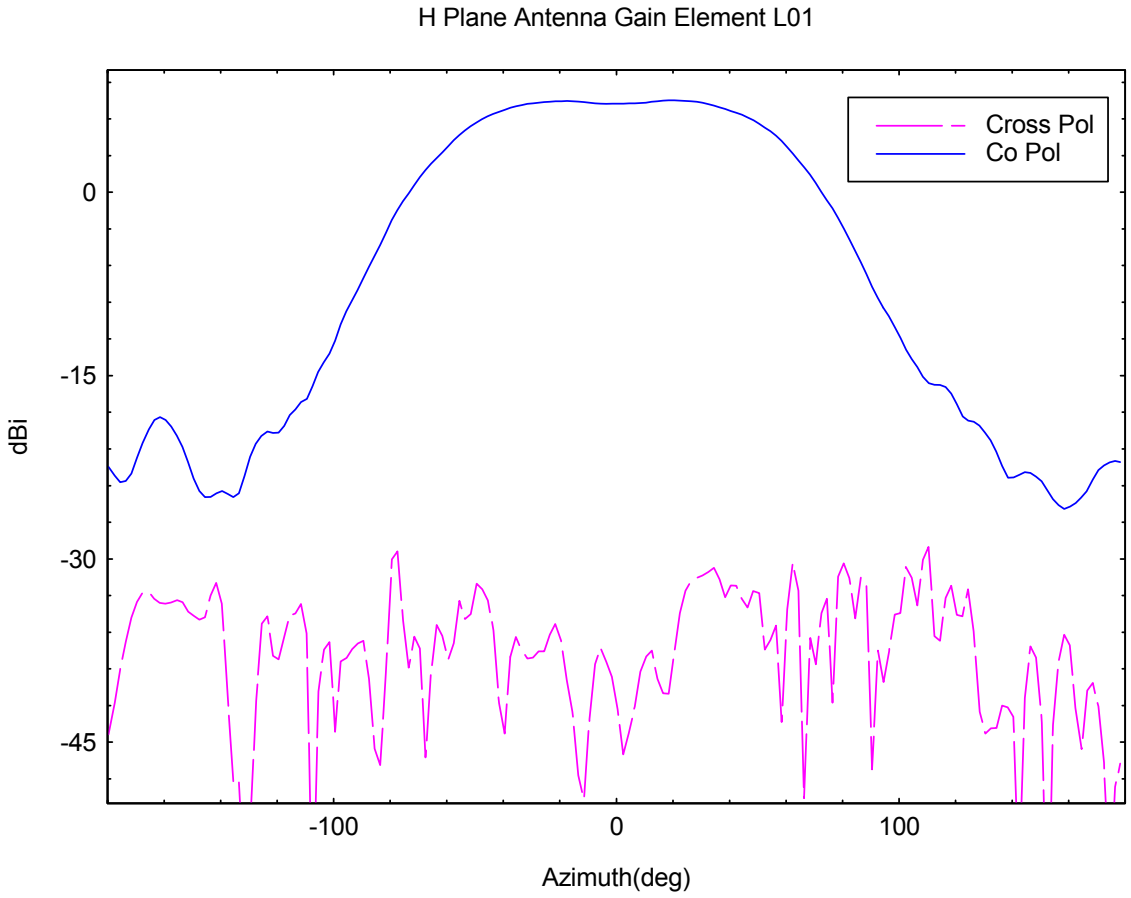

Figure 11. H-plane co-polarized and cross-polarized antenna patterns for element L01.

7.7 Data Collection Summary

Calibration and transfer function data were collected over a period of several months and multiple tests were conducted to verify that data was repeatable. A data collection summary for all tests is given in Appendix C.

8. TRANSFER FUNCTION AND H MATRIX CALCULATIONS

In the theoretical calculations the antenna elements were treated as identical isotropic radiators and the ground plane was incorporated using the theory of images. The geometry of the antenna array at the OATS is shown in Figure 12.

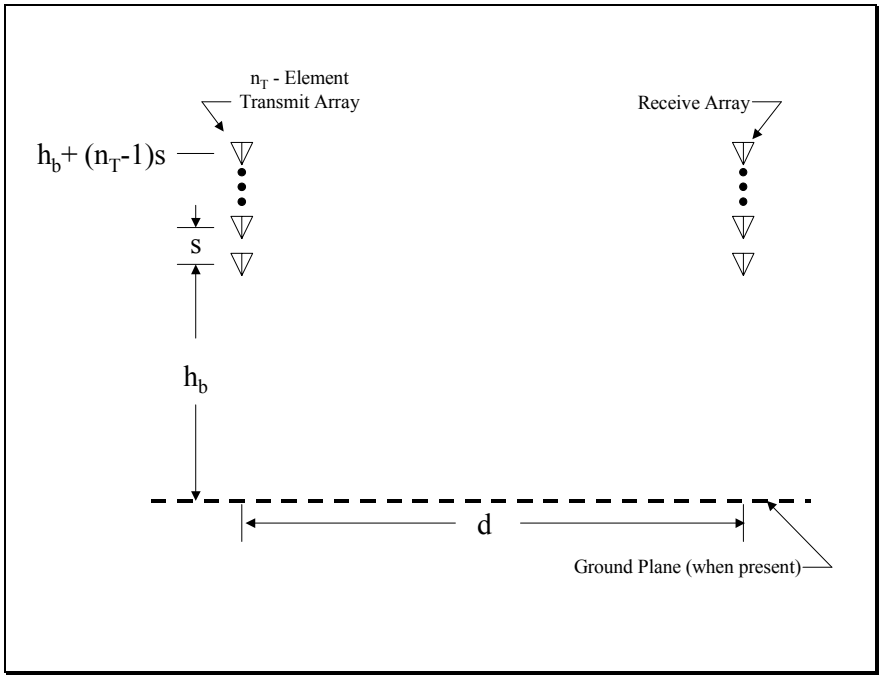

Figure 12. Transmit and receive array geometry.

Here h_b is the height of the bottom antenna element over the ground plane, d is the distance between the arrays and s is the separation between elements. For the tests h_b was 17.5 λ, d was 231.5 λ, and s was λ. Since we are interested in only relative amplitude and phase between antenna elements, the transfer function T_{km} can be simply represented as

$$T_{km} = T\,\frac{e^{-j2\pi r_{km}/\lambda}}{r_{km}}, \tag{5}$$

where $r_{km} = \sqrt{d^2 + (h_k - h_m)^2}$ and h_k and h_m are the transmit and receiver antenna element heights respectively. If we let r'_{km} represent the distance between the k^{th} image source and the m^{th} receiver, then T'_{km}, the image source transfer function (for the reflected path), is

$$T'_{km} = T\,\frac{e^{-j2\pi r'_{km}/\lambda}}{r'_{km}}, \tag{6}$$

with $r'_{km} = \sqrt{d^2 + (h_k + h_m)^2}$. Then if $\tilde{T}_{km}$ is used to represent the transfer function for the direct and reflected signal from the ground plane,

$$\tilde{T}_{km} = T\left(\frac{e^{-j2\pi r_{km}/\lambda}}{r_{km}} + \frac{e^{-j2\pi r'_{km}/\lambda}}{r'_{km}} \right), \tag{7}$$

for vertical polarization, and

$$\tilde{T}_{km} = T\left(\frac{e^{-j2\pi r_{km}/\lambda}}{r_{km}} - \frac{e^{-j2\pi r'_{km}/\lambda}}{r'_{km}} \right), \tag{8}$$

for horizontally polarized signals. **H** is then obtained from $\mathbf{H}=B\tilde{\mathbf{T}}$ with B chosen so that the average of $|\mathbf{H}_{km}|$ over the matrix elements is unity as in Equation 2. The theoretical capacity of the link can now be calculated using Equation 1 and compared with the capacity predicted using the measured channel transfer function.

9. RESULTS

9.1 Transfer Function Identification

Figure 13 shows the magnitude of the measured impulse response from receiver antenna elements 1–16. This is an example of a BLAST 16x16 data set at an early stage of processing. During this test the transmitter and receiver antennas were aligned horizontally. 16 successively delayed orthogonal psuedo-noise codes were simultaneously transmitted from all transmitter elements. The orthogonal coding allowed the signal from each transmitter element to be identified at each receiver antenna as a delayed impulse response. Figure 13 has 16 plots, each with 16 impulses separated by 3.2 μs. Each successive impulse represents the received signal from transmit antennas 1 through 16. Plot 1 is in the upper left hand corner and plot numbers increase from left to right. Row two begins with plot 5, row 3 with plot 9 and row 4 with plot 13. In plot 1, impulse 1 corresponds to the magnitude of the transfer function between transmitter 1 and receiver 1 or $\boldsymbol{T}_{1,1}$. Also on plot 1, impulse 2 corresponds to $\boldsymbol{T}_{2,1}$, impulse 3 to $\boldsymbol{T}_{3,1}$, etc., up to $\boldsymbol{T}_{16,1}$. The first impulse on plot 16 (lower right hand corner) corresponds to $\boldsymbol{T}_{16,1}$, the second impulse to $\boldsymbol{T}_{16,2}$, etc. Since multipath was non-resolvable (the time difference between the direct and reflected signal is less than a chip period), the amplitude of each impulse response forms a lobing pattern (for example, the path length difference between the top transmitter and receiver was 8.95λ, 1.17m or 3.9 ns). Because different transmitter receiver pairs experience fading nulls caused by interference

between the direct and reflected paths, we see the vertical power lobing patterns in the impulse response data. One can see how the lobing pattern changes for different transmitter and receiver combinations by examining the sixteen plots. Note that signals below the peaks of the impulse response represent correlation noise. This data set (Figure 13) contains the 256 transfer functions needed to define the BLAST radio channel and calculate its capacity (C (Bits/Hz/s)). These data are separated into the 256 complex transfer functions, which are then deconvolved using the calibration data. After normalization, **H** is computed in both the time and frequency domains for comparison with the calculated results.

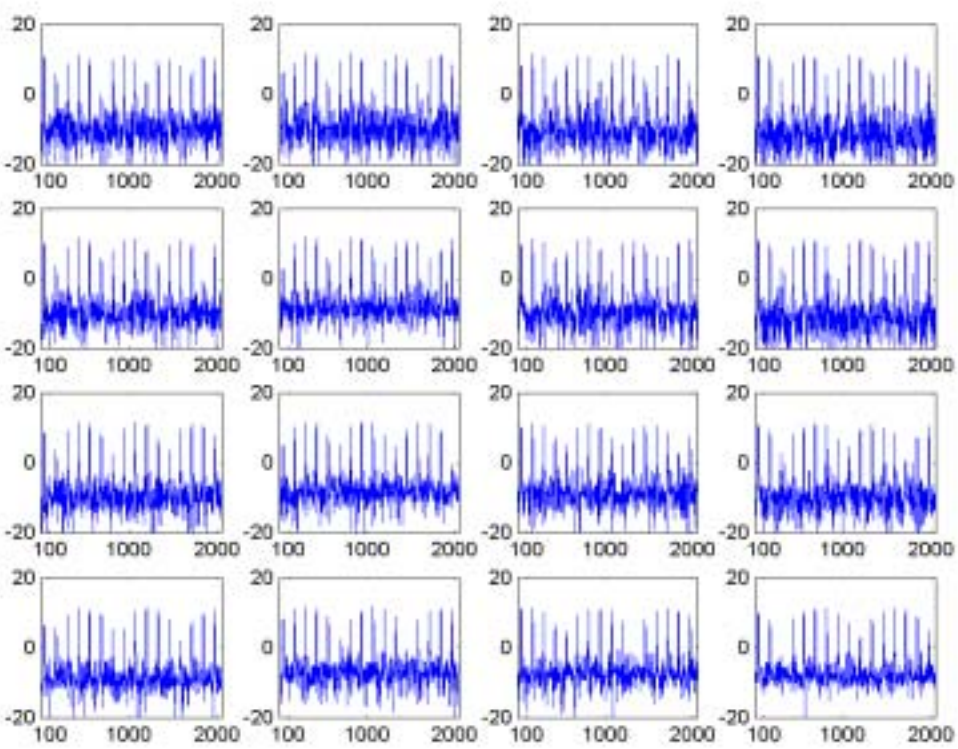

Figure 13. Signals received by 16 antenna elements after correlation. The signals from transmitters 1-16 are seen as delayed impulses. The vertical scale is relative power and measured in dB.

9.2 Theoretical Capacity Calculations

Theoretical capacity curves versus antenna array separation in wavelengths were calculated using the equations in Section 8 for a signal-to-noise ratio (ρ) of 10. Figure 14 and Figure 15 show these results for horizontal and vertical polarization respectively. At small and large separations, capacities with and without the ground plane are similar, although the capacities are much larger at small separations. These results can be understood as follows. Equations (7) and (8) for **T** imply that as the separation *d* becomes

vanishingly small, the diagonal elements become infinite and the off-diagonal elements remain finite. Thus, **T** is proportional to **I** (the identity matrix). Using Equation (2) to normalize **H**, and substituting into Equation (1), it is easy to see that in this limit the capacity is given by $C = n \log_2(1 + \rho)$. Similarly, as *d* becomes infinite, all propagation paths (both direct and reflected) between all transmitters and all receivers become identical. Thus, all the elements of **H** (both diagonal and off-diagonal) approach unity. Again substituting into Equation (1), it can be shown that the capacity in this limit is given by $C = \log_2(1 + n\rho)$. These results imply that for $n = 16$ and $\rho = 10$, the capacities for both polarizations approach *55.4 bits/Hz/s* and *7.3 bits/Hz/s* for small and infinitely large separations, respectively. At intermediate separations the capacity curves interpolate between these two limits. As we move beyond 20λ separation, the capacity without the ground plane drops relative to the capacity with a ground plane present. Now nulls caused by the reflected signal cause off diagonal elements to become small again. This caused the capacity with the ground plane to be greater than without the ground. It was in this region that our tests were performed. The capacities at $d=231.5\ \lambda$ (test separation) are marked on the curves for comparison with the measured results. We see that the curves for vertical and horizontal polarization are similar and that the capacities of the channel at the test antenna separation are almost equal.

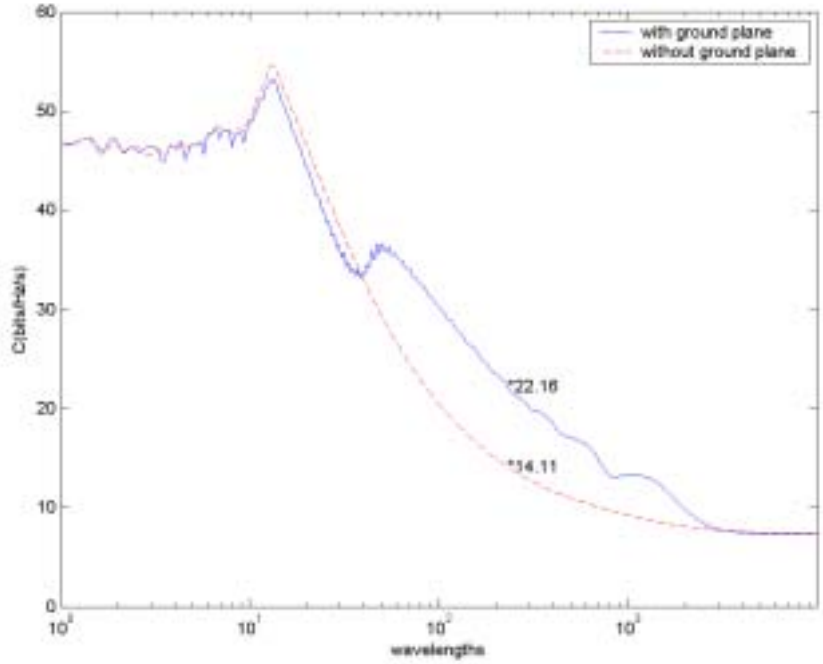

Figure 14. Capacity calculated for the 16x16 BLAST array with and without ground plane. Capacity is for horizontal polarization and ρ=10. The predicted capacity with ground plane at d= 231.5 is 22.16.

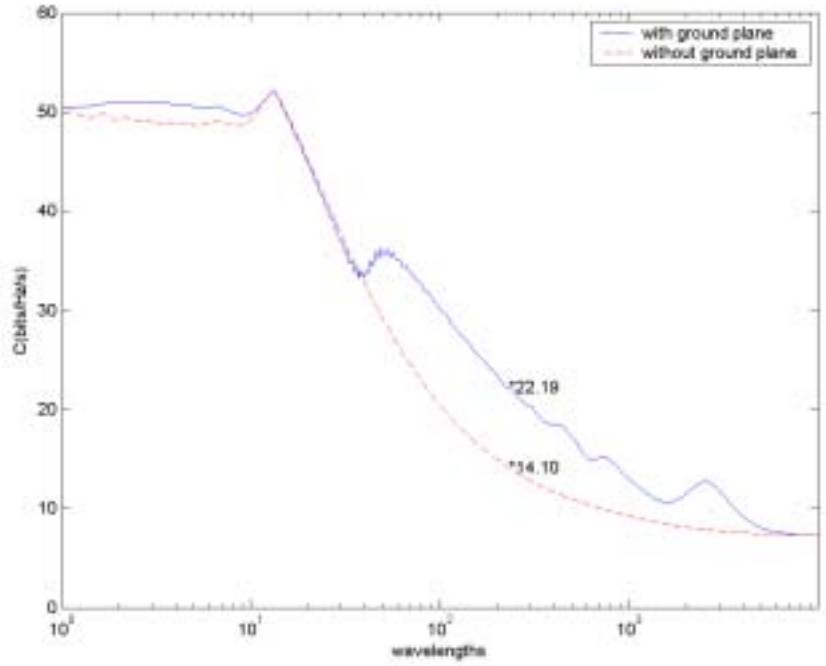

Figure 15. Capacity calculated for the 16x16 BLAST array with and without ground plane. Capacity is for vertical polarization and ρ=10. The predicted capacity with ground plane at d= 231.5 is 22.19.

9.3 Power Lobing Patterns

In addition to the wideband **H** matrix measurements, a series of narrowband measurements were taken for comparison with the wideband results. The CW data was not collected using simultaneous transmission as in the wideband case. Instead single tones were transmitted and received one antenna pair at a time using a signal generator and spectrum analyzer.

Figure 16 shows the theoretical lobing patterns for horizontal antenna polarization. Measured CW data, time domain impulse peak data, and frequency domain data from the wideband measurements are also displayed on this figure. These CW data are labeled using blue circles. The impulse peak data (H_t) were collected using the wideband system with simultaneous transmissions on all transmitter elements. The impulse peaks, black stars, can be extracted from the received signals at each receiver element as described in Section 9.1 and shown in Figure 13. The wideband frequency domain data (H_w) from this graph are then obtained from the impulse data by time shifting the impulse peaks, zero filling to interpolate and remove the unwanted peaks beyond 3.2 μs, and then Fourier transforming the results. The frequency data used for this analysis was one step from the center frequency of the impulse spectrum. This frequency was chosen to avoid possible feed-through at the carrier frequency. These data are displayed as purple diamonds. These data points also represent measured transfer functions between antenna elements before

normalization. The blue line is the lobing pattern calculated at a fine spacing so we can see the curve shapes.

The general trends in these patterns, such as the alignment of lobes seen as a function of elevation (receiver #) versus transmitter, can be seen. We see a good comparison between the calculated lobing pattern and the CW and H_w frequency domain data in these general trends. A similar plot for the vertically polarized antennas is given in Figure 17 (on Figure 17 the CW data is not displayed because it was only collected for 3 transmitters). We also see that the vertically polarized measured data follows the general trends predicted by the calculated curves. A close comparison of plots 16 and 17 shows that the nulls and peaks for the horizontally polarized test are 180 degrees out of phase with the vertically polarized test, as expected from Equations 7 and 8.

However, if we look at the data in more detail we see that the impulse peak fit is less accurate near the signal nulls than the CW or H_w data. This can be seen more easily in Figure 18 which shows the lobing patterns for only 4 transmitters: 1, 2, 3, and 16 (h = 32.5 λ, 31.5 λ, 30.5 λ, 17.5 λ). The difference in fit is caused by a combination of problems when using the time domain results. Some of the error is due to system non-linearity caused by local oscillator feed-through and port-to-port mixer coupling. These effects are filtered out in the frequency domain data, hence the better fit. Figure 19 shows a more detailed view of the data fit for the vertical polarized data. Here we only show plots for the 3 transmitters that had CW data. Another noticeable effect is that the data does not fit equally well for all transmitters. This fit can be adjusted by tweaking the model parameters for antenna element positioning errors. We adjusted the distance between antenna arrays and height of the arrays above the ground plane by .01 to 0.1 λ to obtain the best fit. This was done visually and a least squares approach may have been more accurate, but it was felt the fit was good enough given the number of parameters that may have affected the fit such as gain variations between array elements, array tilt, array height, array rotation etc. Another effect that changes the data fit that can be mitigated in the frequency domain is a shift in the position of nulls as a function of frequency.

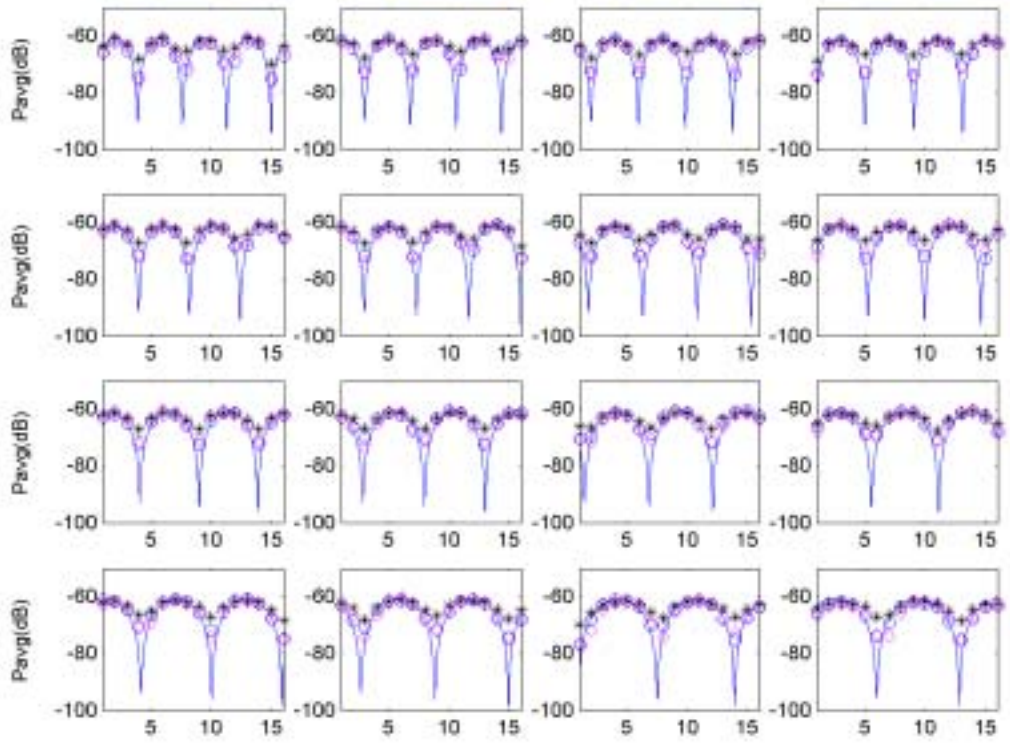

Figure 16. Power lobing patterns versus receiver number for horizontal antenna polarization. Patterns are measured and calculated received power for transmitter 1 to receivers 1-16, top left, transmitter element 4 to receivers 1-16, top right, transmitter 13, bottom left, and transmitter 16, bottom right. Transmitter 1 was the upper transmit element at an elevation of 32.5 λ above the ground plane. On the graphs, blue circles are CW, black stars are impulse peaks, and purple diamonds are frequency domain data.

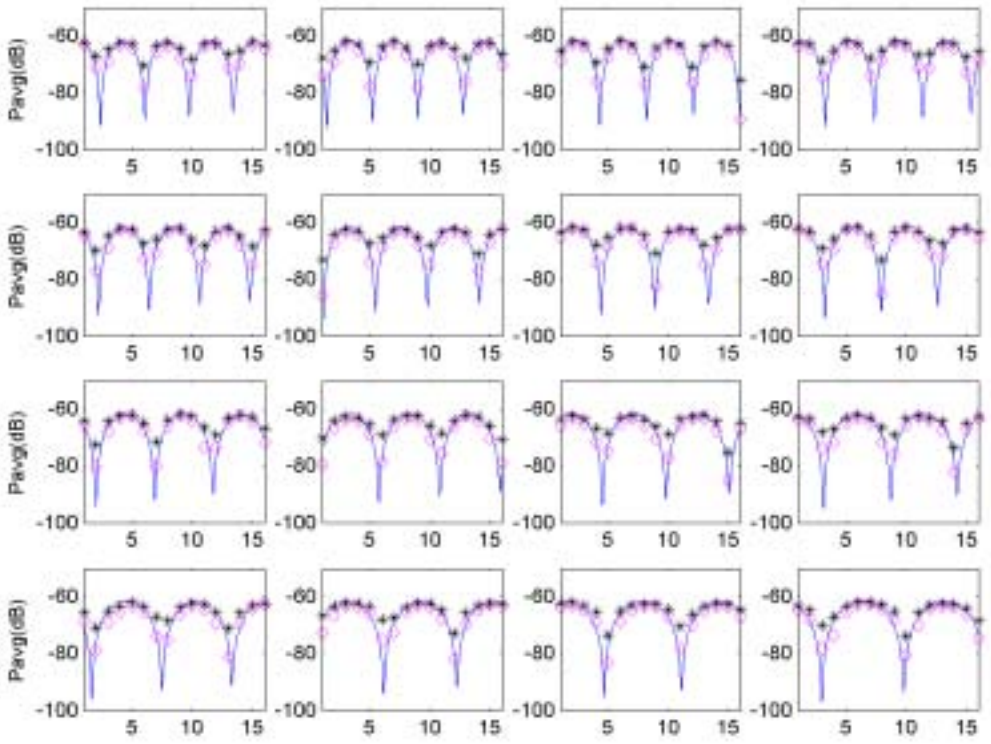

Figure 17. Power lobing patterns versus receiver number for vertical antenna polarization. Patterns are measured and calculated received power for transmitter 1 to receivers 1-16, top left, transmitter element 4 to receivers 1-16, top right, transmitter 13, bottom left, and transmitter 16, bottom right. Transmitter 1 was the upper transmit element at an elevation of 32.5 λ above the ground plane. On the graphs, black stars are impulse peaks and purple diamonds are frequency domain data.

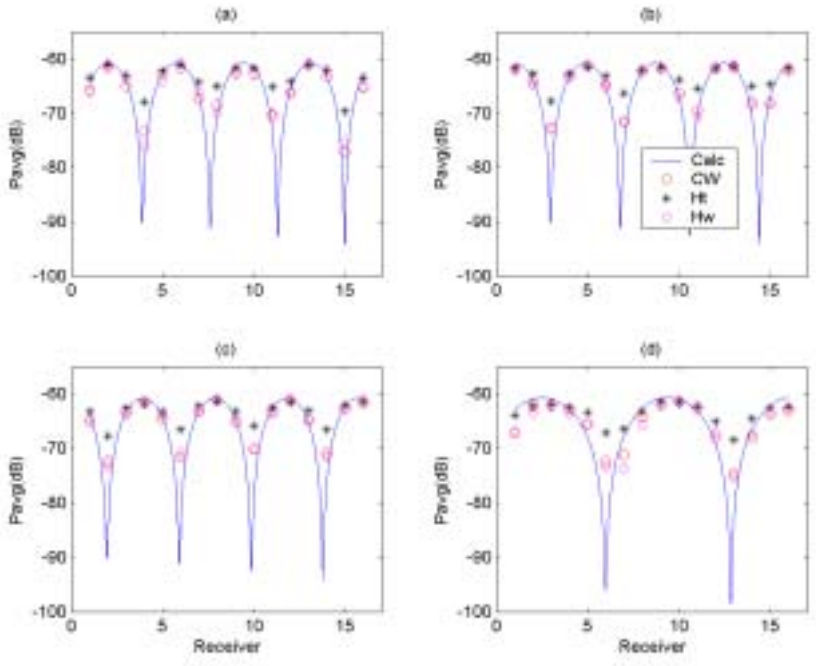

Figure 18. Horizontal polarization power lobing patterns for receivers 1-16 from: (a) transmitter 1, (b), transmitter 2, (c) transmitter 3, (d) transmitter 16. Transmitter 1 is on the top of the array at 32.5 λ above the ground plane. Receiver 0 is also on the top at 32.5 λ above the ground plane.

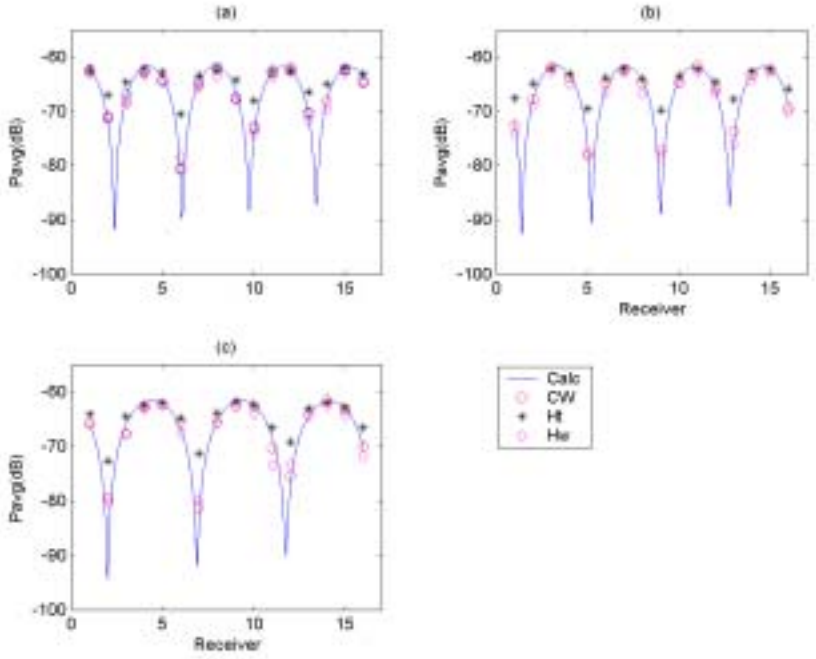

Figure 19. Vertical polarization power lobing patterns for receivers 1-16 from: (a) transmitter 1, (b), transmitter 2, (c) transmitter 3, (d) transmitter 9. Transmitter 1 is on the top of the array at 32.5 λ above the ground plane. Receiver 0 is also on the top at 32.5 λ above the ground plane.

We can see these frequency effects for horizontal polarization by using Equation 7. An analysis of null shifting at three frequencies is shown in Figure 20. This graph shows the dB power fluctuation near receiver antenna element 4 for a signal from transmitter element 17. Although a 20-MHz shift in frequency can cause a 14.6-dB fade to decrease to only an 8.2-dB fade (which is on the order of the observed deviations from narrow-band), the results should be averaged over the bandwidth (depending on how the wide band impulse peak fluctuations are observed in the recordings). Therefore the shift in null location with frequency seems to come up short as the sole explanation for the impulse-peak deviations from the narrowband results. An examination of the frequency domain measurement results indicated that LO feed-through is also a contributing factor for errors at null locations. It was concluded that the combination LO feed-through and null shifting as a function of frequency are responsible for errors when comparing the narrowband calculations to the wideband time domain data. Since there is no easy way to remove this effect in the time domain, the **H** matrix and capacity calculation comparisons were done in the frequency domain where these effects could be filtered out.

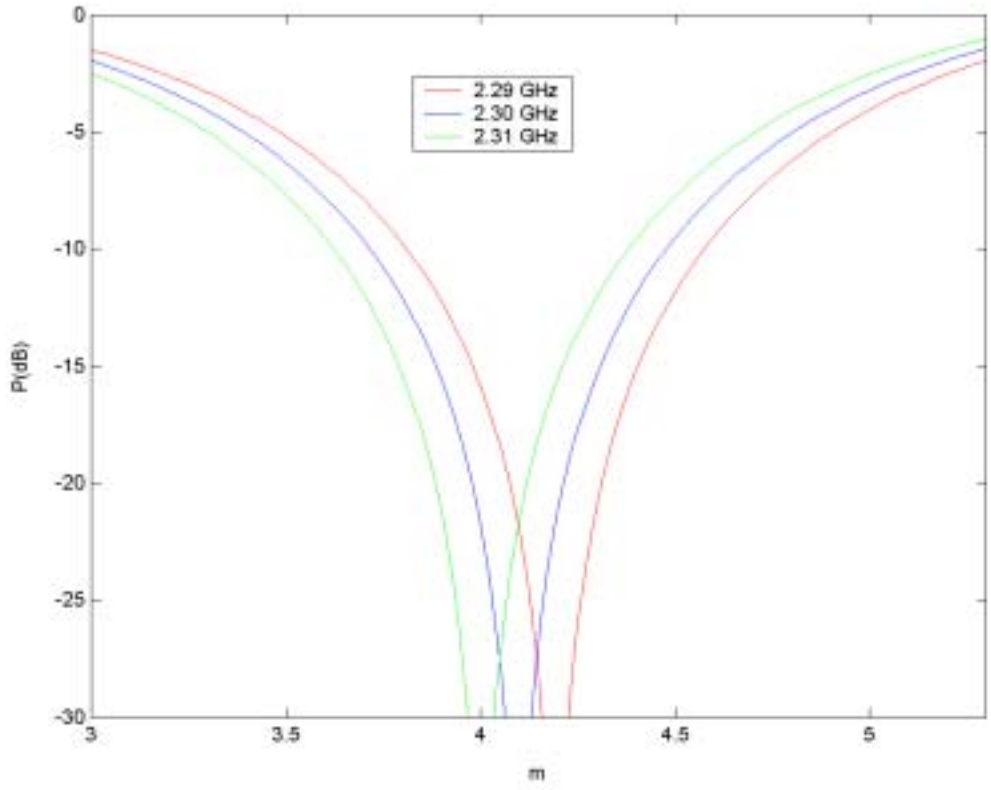

Figure 20. Frequency effect on null location versus receive antenna height, red for f = 2.29 GHz, blue for f = 2.3 GHz, green for f = 2.31 GHz.

In this analysis, we use d = 231.5 wavelengths at center frequency and h_b = 17.25 center frequency wavelengths.

9.4 Comparison of Measured and Predicted Results

Using Equations 7 and 8, **H** was calculated and compared to the measurement results for both horizontal and vertical polarization. Figure 21 shows a surface plot of the calculated and measured results for both magnitude and phase. It was found that the measured phase results did not agree well with the predictions, presumably due to quadrant errors that we were unable to resolve.

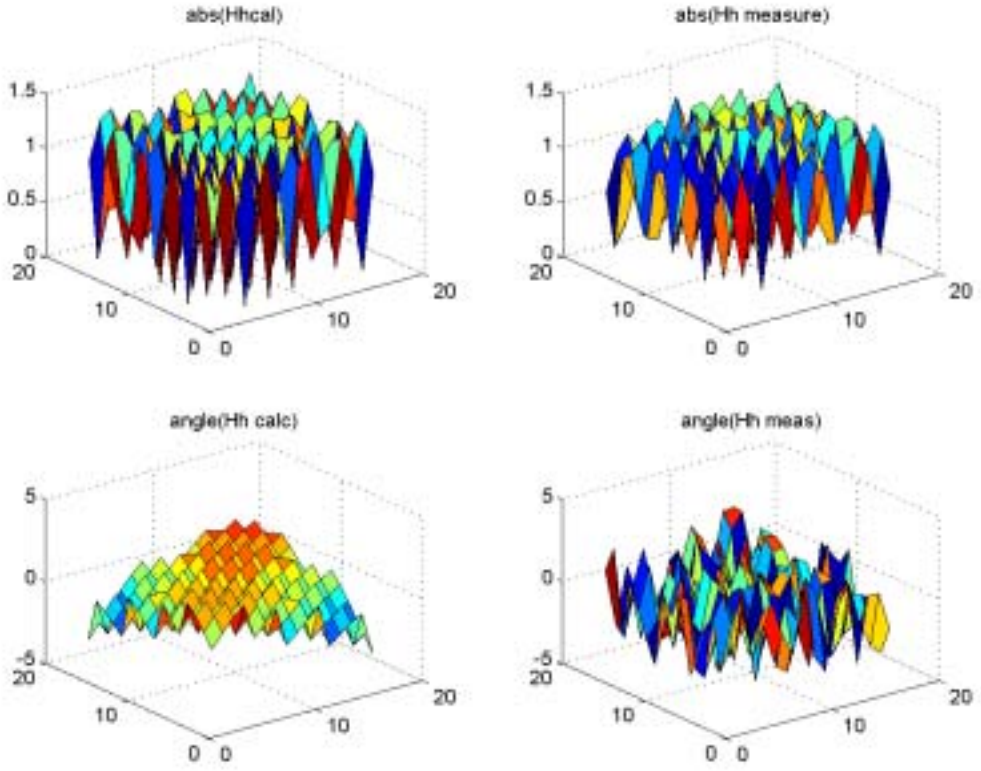

Figure 21. Magnitude (abs) and phase (angle) surface plots of the measured and calculated H matrix. The vertical scale is in linear units and the phase is measured in radians. The horizontal scale is the *i,j* index of H.

The error in the magnitude of **H** was evaluated using the following equations:

$$\varepsilon_{ij} = \left|H_{ij}^{\ calc}\right| - \left|H_{ij}^{\ meas}\right|, \tag{9}$$

$$\bar{\varepsilon} = \frac{1}{n_t n_r} \sum_{ij} \varepsilon_{ij} \ , \tag{10}$$

$$\text{var}(\varepsilon) = \frac{1}{n_t n_r} \sum_{ij} \left(\varepsilon_{ij} - \bar{\varepsilon}\right)^2 , \tag{11}$$

$$\sigma_\varepsilon = \sqrt{\text{var}(\varepsilon)} . \tag{12}$$

Using Equation 1 the capacity was calculated for a system ρ=10 for both the horizontally polarized and vertically polarized cases using the measured **H** matrix and the calculated **H** matrix.

The statistical comparisons between the **H** matrices are given in Table 1 and Table 2. We see from Table 1 that the variance of the difference in magnitudes between **H** measured and **H** calculated was 0.026 and 0.023 for the horizontal and vertical polarization cases respectively. In Table 2 we see the error between the capacity calculated using the measured **H** and the theoretical **H** was 5% for horizontal polarization and 0.27% for vertical polarization. Larger errors for the horizontal polarization case may be due to mutual antenna coupling which was ignored in the calculations and was stronger for the horizontal polarization case.

Table 1. Difference between Measured and Calculated **H** Matrix for 16x16 Element Array over NIST Ground Plane

	$\bar{\varepsilon}$	var(ε)	σ_ε
H Polarization	-0.0376	0.0260	0.16
V Polarization	-0.0084	0.0230	0.15

Table 2. Measured and Theoretically Predicted Channel Capacities for 16x16 Element Array over NIST Ground Plane for ρ =10

	C_{calc}(b/Hz/s)	C_{meas}(b/Hz/s)	ΔC (b/Hz/s)	% Error
H Polarization	22.16	21.04	1.12	5
V Polarization	22.19	22.25	0.06	0.27

Since it was known that small changes in transmitter separation and array height could change the **H** matrix, a parameter study was done to evaluate the effects of array positioning errors. The results of this parameter study relating receiver antenna array height and transmitter to receiver separation versus channel capacity is shown in Figure 22. We can see that changes in separation (*d)* on the order of 1λ and in *hmax* on the order of 0.1λ will only cause changes in *C* on the order of 0.1 Bits/Hz/s.

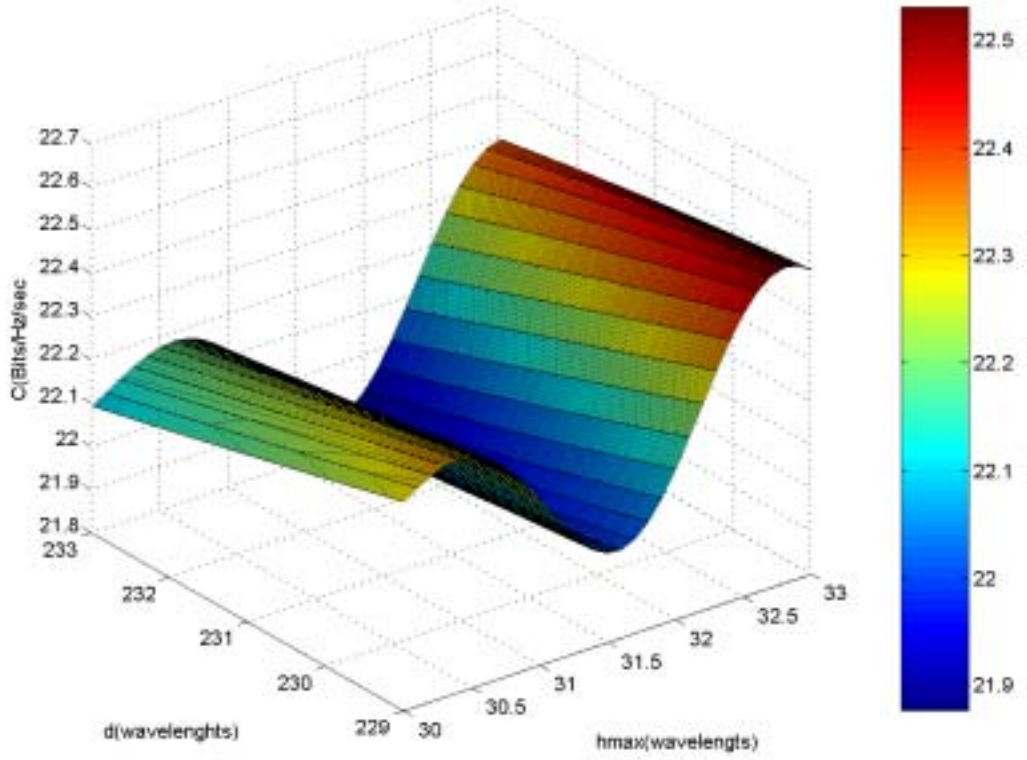

Figure 22. The capacity of a 16x16 element array situated over a ground plane versus the antenna array separation (d), and the height above the ground plane of the top element of the receiving array (hmax).

10. CONCLUSIONS

A 16-channel MIMO antenna system for simultaneous measurement of the BLAST channel transfer function was developed. It utilized a wideband maximal sequence-coding scheme to identify different radio paths between antenna elements. A methodology was implemented for analyzing the accuracy of transfer function estimates and predicted channel capacity based on the channel response (**H** matrix) measurements using the NIST OATS and RF analysis of the radiowave propagation environment. The variance of the magnitude difference between the measured and calculated H matrix was between 0.023 and 0.026. The difference between the channel capacity calculated using the measured **H** and the theoretical **H** was between 0.27% and 5%.

The experiment demonstrated that a wideband system accurately measured the **H** matrix. This measurement is necessary for prediction of the channel capacity. The 16-element MIMO antenna system was also shown to behave as predicted by the model developed to calculate the channel transfer functions in Section 9.

11. REFERENCES

1. G. J. Foschini, "Layered space-time architecture for wireless communication in a fading environment when using multiple antennas," *Bell Labs Technical Journal*, Vol. 1, No. 2, pp. 41-59, Autumn 1966.

2. G. J. Foschini and M. J. Gans, "On limits of wireless communications in a fading environment when using multiple antennas," *Wireless Personal Communications*, Kluwer Academic Publishers, Vol. 6, 1998, pp. 311-335.

3. S. Verdu and S. Shamai, "Spectral efficiency of CDMA with random spreading," *IEEE Transactions on Information Theory*, Vol. 45, No. 2, pp. 622-640, Mar. 1999.

4. P. Wilson, P. Papazian, M. Cotton and Y. Lo, "Advanced antenna test bed characterization for wideband wireless communications," NTIA Report 99-369, Aug. 1999.

5. D. Chizhik, G. J. Foschini, and R. A Valenzuela, "Capacities of multi-element transmit and receive antennas: Correlations and keyholes," *Electronics Letters*, Vol. 36, No. 13, pp. 1099-1100, Apr. 2000.

6. D. Chizhik, J. Ling, P. Wolinsky, R. Valenzuela, N. Costa, and K. Huber, "Multiple input multiple output measurements and modeling in Manhattan," in *Proc*. *IEEE Fall 2002 Vehicular Technology Conference,* Vancouver, B.C., Canada, Sep. 24 -29, 2002.

APPENDIX A: ANTENNA COUPLING DATA SUMMARY TABLES

Coupling data is summarized using the following convention: Anum1, num2 = S (dB), where num1 = antenna element connected to port 1, num2 = antenna element connected to port 2.

Table A-1.Vertical Antenna Coupling Summary

Measurement	**File#**	**Disk#**	**S_{21} @ CF**				**Comments**
			Amp(dB)	±	**Phase°**	±	
Cable(1,2)							
Cal1-thru	00	1	-0.5		-0.7		
A1,2	01		-31.5		-58		
A1,3	02		-52.5		102.7		
A1,4			-51.4		146.3		
A1,5	03		-53.4		162		
A1,6	04		-57.8		146		
A1,7	05		-54		133		
A1,8	06		-54		147		
A1,9	00	2	-56		153		
A1,10	01		-57		169		
A1,11	02		-62		-178		
A1,12	03		-78		92		
A1,13	04		-67		146		
A1,14	05		-65	5	76		
A1,15	06		-70	7.5			
A1,16	00	3	-70	10	-175		
A1,2	01		-31.5	0.2	-58		Repeat
A1,3	02		-52	0.5	105		Repeat
A1,4	03		-51	0.5	150		Repeat
A1,5	04		-53	1	164		Repeat
A1,6	05		-58	2	147		Repeat
A1,7	06		-60	5	132		Repeat
Cable(2,3)							
Cal2-thru	00	4	0.1	0	-0.1	0	
A2,3	01		-32	0.15	-54	6	
A2,4	02		-50	1.5	105	15	
A2,5	03		-50	2	150	15	
A2,6	04		-53	2			
A2,7	05		-58	4	180	50	
A2,8	06		-57	3	130	20	
A2,9	00	5	-56	1.5	140	20	
A2,10	01		-57	1.5	0	30	0 indicates phase
A2,11	02		-58	4	0	301	crosses 0,180°
A2,12	03		-65	10	0	50	boundary

A2,13	04		-65	10	0	50	
A2,14	05		-70	10	0	100	
A2,15	06		-75	15	0	50	
A2,16	00	6	-66	2	0	50	
Cable(3,4)							
Cal3-thru	01						
A3,4	02		-31.7	0.1	54	6	
A3,5	03		-49.5	1	110	10	
A3,6	04		-50	2	145	10	
A3,7	05		-53	2	155	15	
A3,8	06		-57	1	140	15	
A3,9	00	7	-56	1.5	130	20	
A3,10	01		56	3	140	30	
A3,11	02		56	4	0	25	
A3,12	03		60	8	0	25	
A3,13	04		-58	5	0	25	
A3,14	05		-70	10	0	25	
A3,15	06		-66	5	0		
A3,16	00	8	-66	6	0		
Cable(4,5)							
Cal4-thru	01		0.01	0.002	0.07	0.01	
A4,5	02		-32	0.3	-54	6	
A4,6	03		-49.5	1.5	105	15	
A4,7	04		-49.5	0.75	145	10	
A4,8	05		-52	1	160	20	
A4,9	06		-57	2.5	150	20	
A4,10	00	9	-56	4	140	30	
A4,11	01		-54	3	0		
A4,12	02		-58	4	0		
A4,13	03		-55	2	0		
A4,14	04		-62	3	0		
A4,15	05		-62	3	0		
A4,16	06		-65	10	0		
Cable(5,6)							
Cal5-thru	00	10	0.005		-0.759		Bad data
Cal6-thru	01		0.025		-0.0206		
A5,6	02		-32	0.15	-56	5	
A5,7	03		-49	0.4	105	10	
A5,8	04		-50	1	145	12	
A5,9	05		-52	2	0		
A5,10	06		-58	3	0		
A5,11	07		-53	3	140	15	
A5,12	00	11	-54	4	150	25	
A5,13	01		-51	2	0		
A5,14	02		-58	2	0		
A5,15	03		-60	4	0		

A5,16	04		-67	6	0		
Cable(6,7)							
Cal7-thru	05						
A6,7	06		-31.9	0.1	-56	4	
A6,8	00	12	-50	2	105	10	
A6,9	01		-50	2	150	16	
A6,10	02		-52	2	0		
A6,11	03		-56	4	150	25	
A6,12	04		-58	4	130	25	
A6,13	05		-53	1.5	140	20	
A6,14	06		-56	1.5	0		
A6,15	00	13	-60	4	0		
A6,16	01		-63	5	0		
A7,8	02		-32	0.2	-54	5	Use cable 6, 7
A7,9	03		-47	2	110	15	
A7,10	04		-48	1.5	140	15	
A7,11	05		-50	1.5	150	20	
A7,12	06		-54	2	150	20	
A7,13	00	14	-55	1	140	15	
A7,14	01		-55	1.5	140	25	
A7,15	02		-56	3	0		
A7,16	03		-60	5	0		
A8,9	04		-31.9	0.2	-54	6	
A8,10	05		-50	1	110	10	
A8,11	06		-50	1	140	12	
A8,12	00	15	-51	0.75	160	15	
A8,13	01		-57	1.5	150	20	
A8,14	02		-56	2.5	140	30	
A8,15	03		-56	2.5	140	30	
A8,16	04		-58	2.5	0		
A9,10	05		-32	0.15	-56	6	
A9,11	06		-49	0.5	105	10	
A9,12	00	16	-49	0.75	145	15	
A9,13	01		-52	1.5	160	20	
A9,14	02		-58	3	0		
A9,15	03		-58	3	140	30	
A9,16	04		-56	3	140	30	
Cable(10,11)							
Cal8-thru	05						
A10,11	06		-31.9	0.15	-54	4	
A10,12	00	17	-50	1.25	105	15	
A10,13	01		-50	1.5	140	20	
A10,14	02		-53	2.5	0		
A10,15	03		-55	4	0		

A10,16	04		-58	4	140	25	
A11,12	05		-31.8	0.2	-54	5	Use cable 10, 11
A11,13	06		-50	2	110	15	
A11,14	00	18	-50	2	140	20	
A11,15	01		-53	2	0		
A11,16	02		-60	4	0		
A12,13	03		-32	0.25	-52	5	Use cable 10, 11
A12,14	04		-48.5	2	110	15	
A12,15	05		-50	2	140	15	
A12,16	06		-53	2	0		
A13,14	00	19	-31.9	0.25	-56	5	Use cable 10, 11
A13,15	01		-50	1.25	105	10	
A13,16	02		-51	1.5	145	15	
A14,15	03		-31.9	0.2	-56	5	Use cable 10, 11
A14,16	04		-52	1.5	95	13	
A15,16	05		-31.4	0.2	-56	5	Use cable 10,11

Table A-2. Horizontal Antenna Coupling Summary

Measurement	**File#**	**Disk#**	**S_{21} @ CF**				**Comments**
			Amp(dB)	±	**Phase°**	±	
Cable(1,2)							
Cal1-thru	00	20	0	0.005	-0.100	0.020	
A1,2	01		-22.8	0.15	170	6	
A1,3	02		-31.8	0.4	170	8	
A1,4	03		-37.0	6	0		
A1,5	04		-42.2	0.6	0		
A1,6	05		-45.6	0.5	0		
A1,7	06		-48.5	1.5	0		
A1,8	00	21	-50	2	0		
A1,9	01		-54	2	0		
A1,10	02		-56	3	0		
A1,11	03		-56	4	0		
A1,12	04		-58	2	0		
A1,13	05		-60	1	0		
A1,14	06		-65	7.5	0		
A1,15	00	22	-70	20	0		
A1,16	01		-65	10	0		
Cable(1,2)							
Cal2-thru	02		-0.35	0.0	0.74		

A2,3	03		-22.6	0.2	166	6	
A2,4	04		-31.4	0.4	170	6	
A2,5	05		-37	0.4	0		
A2,6	06		-42	1	0		
A2,7	00	23	-45	1.5	0		
A2,8	01		-48	2	0		
A2,9	02		-50	2.5	0		
A2,10	03		-52	2.5	0		
A2,11	04		-54	2	0		
A2,12	05		-56	1	0		
A2,13	06		-56	2	0		
A2,14	00	24	-60	10	0		
A2,15	01		-70	15	0		
A2,16	02		-70	12	0		
Cable(1,2)							
Cal3-thru	03		-0.35	0.0	3.9	0.020	
A3,4	04		-22.4	0.1	170	6	
A3,5	05		-31.4	0.2	170	8	
A3,6	06		-37	0.1	170	10	
A3,7	00	25	-42	1.3	0		
A3,8	01		-45	1.5	0		
A3,9	02		-48	2	0		
A3,10	03		-50	2	0		
A3,11	04		-52	0.1	0		
A3,12	05		-54	2	0		
A3,13	06		-56	4	0		
A3,14	00	26	-60	10	0		
A3,15	01		-70	12.5	0		
A3,16	02		-70	17	0		
Cable(1,2)							
Cal4-thru	03		-0.7	0	.66		
A4,5	04		-22.6	0.2	168	6	
A4,6	05		-31.4	0.4	170	10	
A4,7	06		-37	0.5	0		
A4,8	00	27	-41	1	0		
A4,9	01		-45.5	1	0		
A4,10	02		-48	1	0		
A4,11	03		-50	1	0		
A4,12	04		-52	2	0		
A4,13	05		-54	5	0		
A4,14	06		-60	7.5	0		
A4,15	00	28	-60	7.5	0		
A4,16	01				0		
Cable(1,2)							
Cal5-thru	02		-0.05	0	-0.0206	0	
A5,6	03		-22.6	0	164	6	

A5,7	04		-31.4	0.2	165	10	
A5,8	05		-37	0.4	0		
A5,9	06		-41	0.4	0		
A5,10	00	29	-45	0.4	0		
A5,11	01		-48	1	0		
A5,12	02		-50	2	0		
A5,13	03		-52	4	0		
A5,14	04		-56	4	0		
A5,15	05		-58	5	0		
A5,16	06		-58	5	0		
Cable(1,2)							
Cal7-thru	00	30	-0.08	0	0.439	0	
A6,7	01		-22.5	0.2	0.166	6	
A6,8	02		-31.5	0.3	170	5	
A6,9	03		-37	0.3	0		
A6,10	04		-42	0.7	0		
A6,11	05		-45	1.5	0		
A6,12	06		-48	2	0		
A6,13	00	31	-50	2.5	0		
A6,14	01		-52	2.5	0		
A6,15	02		-54	3	0		
A6,16	03		-57	2	0		
Cable(1,2)							
Cal8-thru	04		-0.01	0	-1.4	0	
A7,8	05		-22.6	0.1	168	6	
A7,9	06		-31.6	0.4	170	8	
A7,10	00	32	-37	0.5	0		
A7,11	01		-42	0.5	0		
A7,12	02		-45	1.5	0		
A7,13	03		-47	2	0		
A7,14	04		-50	2	0		
A7,15	05		-52	1.5	0		
A7,16	06		-55	0.75	0		
Cable(1,2)							
Cal9-thru	00	33	-0.07	-3.2	0		
A8,9	01		-22.5	0.2	170	6	
A8,10	02		-31.5	0.5	170	10	
A8,11	03		-37	1	0		
A8,12	04		-42	1	0		
A8,13	05		-45	1.5	0		
A8,14	06		-48	1.5	0		
A8,15	00	34	-50	1	0		
A8,16	01		-52	0.4	0		
Cable(1,2)							
Cal10-thru	02		-0.09	0	-1.7	0	

A9,10	03		-22.6	0.2	162	6	
A9,11	04		-31.4	0.4	165	10	
A9,12	05		-37	0.5	0		
A9,13	06		-41.5	0.75	0		
A9,14	00	35	-45	0.5	0		
A9,15	01		-47.9	0	0		
A9,16	02		-50.5	0.75	0		
Cable(1,2)							
Cal11-thru	03		-0.1	0	-1.8	0	
A10,11	04		-22.6	0.15	166	6	
A10,12	05		-31.4	0.5	170	9	
A10,13	06		-37	0.4	0		
A10,14	00	36	-41.8	0.2	0		
A10,15	01		-45.5	0.1	0		
A10,16	02		-48.5	0.1	0		
Cable(1,2)							
Cal12-thru	03		-0.1	0	-1.64	0	
A11,12	04		-22.5	0.1	168	6	
A11,13	05		-31.4	0.2	170	7.5	
A11,14	06		-37	0.4	0		
A11,15	00	37	-42	1	0		
A11,16	01		-46	1	0		
Cable1,2							
Cal13-thru			-0.11	0	-2.8		
A12,13	02		-22.6	0.1	164	6	
A12,14	03		-31.5	0.2	165	8	
A12,15	04		-37.2	0.5	0		
A12,16	05		-42.5	0.1	0		
Cable(1,2)							
Cal13-thru			-0.1	.700			
A13,14	06		-22.6	0.2	164	4	
A13,15	00	38	-31.6	0.4	165	10	
A13,16	01		-37.6	0.6	0		
Cable(1,2)							
Cal15-thru			-0.1	0	-4.9	0	
A14,15	02		-22.6	0.15	162	6	
A14,16	00	39	-32	0.4	165	10	0
Cable(1,2)							
Cal16-thru			-0.12	0	-1.76	0	
A15,16	01		-22.9	0.1	164	6	

APPENDIX B: ANTENNA ELEMENT CALIBRATION SUMMARY TABLES

Table B-1. E/H Co-polarized and Cross-polarized Antenna Scans for Element L01

File	Type	Description
ITS01	E/H co/cross scan data	Element L01
ITS01b	E/H co/cross scan data	Repeat after 2 hours
ITS01c	E/H co polarized	Bore-sight Freq. Scan

Table B-2. Summary of E and H Scan Co-polarized Antenna Element Calibration Data. Bore-sight Gain and Phase at 2300 MHz for Each Element and Range Calibration Files

Bore-sight Gain and Phase			Antenna Element Calibration Data				
Ant file	v phase (deg)	h phase[1] (deg)	v amp (dB)	h amp (dB)	Δv phase[2] (deg)	Δh phase[2] (deg)	Δ v amp[2] (dB)
04/04/2001							
sacal1**							
L01cal1	-52		7.52				
L01	-51.9	127.7	7.51		0.1		-0.01
L02	-53.9	-54.5	7.47		-1.9		-0.05
L03	-53.6	-53.9	7.47		-1.6		-0.05
L04	-52.2	-52.9	7.48		-0.2		-0.04
L05	-53.2	-53.4	7.49		-1.2		-0.03
L01cal2	-52.41		7.46		-0.41		-0.06
sacal2[3]							
04/05/2001							
sacal3[3]	0		16.5				
L01cal2	-74.61		7.6				
L06	-77.4	102.9	7.63	7.61	-2.79		0.03
L07	-75.2	104.5	7.53	7.53	-0.59		-0.07
L08	-74.1	105.9	7.66	7.63	0.51		0.06
L09	-74.7	105.1	7.6	7.61	-0.09		0
L10	-74.63	105.3	7.58	7.57	-0.02		-0.02
L11	-75.21	104.6	7.55	7.56	-0.6		-0.05
L12	-74.09	105.6	7.5	7.49	0.52		-0.1
L01cal4	-73.89		7.56		0.72		-0.04
L13	-73.97	106	7.54	7.53	0.64		-0.06
L14	-75.4	104.3	7.61	7.61	-0.79		0.01
L15	-74.3	105.6	7.52	7.5	0.31		-0.08
L16	-74.1	105.5	7.56	7.56	0.51		-0.04
L17	-75.1	104.72	7.51	7.5	-0.49		-0.09
L18	-74.9	104.81	7.51	7.54	-0.29		-0.09
L19	-74.7	105.4	7.42	7.41	-0.09		-0.18
L20	-74.4	105.6	7.51	7.52	0.21		-0.09

L01cal5	-67.58		7.26		7.03	-0.34	
sacal4[3]	-4.65		16.45				
04/06/2001							
sacal5[3]							
L01cal6	-63.67			7.56			
L21	-64.28	115.51	7.54	7.56	-0.61		0
L22	-58.34	121.15	7.11	7.14	5.33		-0.42
L23	-56.86	123.2	7.09	7.09	6.81		-0.47
L24	-59.15	121.2	7.28	7.22	4.52		-0.34
L25	-54.86	125.2	6.94	6.95	8.81		-0.61
L26	-62.5	117.08	7.61	7.63	1.17		0.07
L27	-60.5	118.7	7.27	7.3	3.17		-0.26
L28	-62.97	116.9	7.53	7.56	0.7		0
L29	-64.69	115	7.52	7.58	-1.02		0.02
L30	-63.59	116.2	7.49	7.52	0.08		-0.04
L31		126.1		6.64			
L31r	-63.37	116.3	7.55	7.59	0.3		0.03
L01cal7	-62			7.55	1.67		-0.01
sacal6[3]							
04/09/2001							
sacal6[3]							
L01cal8	-66.52		7.64				
L32	-67.05	112.85	7.59	7.6	-0.53	-0.05	
L33	-67.36	112.34	7.59	7.61	-0.84	-0.05	
L34	-67.22	112.7	7.55	7.55	-0.7	-0.09	
L35	-66.78	112.9	7.56	7.58	-0.26	-0.08	
L22r	-67.83	112.4	7.54	7.54	-1.31	-0.1	
L23r	-65.36	114.64	7.56	7.58	1.16	-0.08	
L24r	-67.52	112.6	7.53	7.54	-1	-0.11	
L25r	-66.32	113.75	7.51	7.54	0.2	-0.13	
L26r	-66	113.66	7.56	7.56	0.52	-0.08	
L01CAL9	-64.63		7.53		1.89	-0.11	
sacal9[3]							

[1] h phase can be 180° out of phase due to misalignment of calibration horn and antenna test fixture.
[2] Δ phase and Δ amp data are relative to LO1 cal data from the beginning of the measurement set.
[3] range calibration data collected using the range calibrated standard gain horn.

APPENDIX C: DATA COLLECTION SUMMARY

Tables C-1 to C-4 summarize the data collected in this experiment.

Table C-1. Broadband Channel Sounder BLAST Data Files and Data Descriptions

Data Type	Date	Data File	Description
Calibration	5/30/02	377-380.xr	Diagonal TxCal Data, *i=j=1……16.*
Calibration	5/30/02	381-396.xr	RxCal Data, *i=1, j=1……16.*
16x16 BLAST	6/7	663.br	Vertical Polarized Antennas
16x16 BLAST	6/7	665.br	Repeat Vpol Test
1x16 BLAST	6/8	666.br	VPol, Tx=17, Rx=1-16
16x16 BLAST	6/8	667.br	Repeat Vpol Blast after disconnecting Tx cabling and moving Tx overnight.
16x16 BLAST	6/8	668.br	Repeat Vpol Blast after removing timing cable which was left on ground plane.
1x16 BLAST	6/13	672,673,674.br	HPol, Tx=17 Rx = all, repeat after computer malfunction.
1x16 BLAST	6/13	675-689.br	HPol, Tx=18,19…….32 Rx=all
16x16 BLAST	6/14	690,691.br	Repeat Hpol BLAST twice.
Keyhole Test	6/14	692.br	HPol, splitter feeds Rx A1 to all channels
1x16 BLAST	6/15	693-708.br	VPol Tx=17,18…..32
16x16 BLAST	6/15	710.br	VPol, transmitter cables reversed data does not repeat, discard.
Keyhole Test	6/15	711.br	VPol, splitter feeds Rx A1 to all channels.
16x16 BLAST	6/16	713.br	VPol repeat after cables reset.
16x16 BLAST	6/16	714.br	VPol repeat
16x16BLAST	6/18	715.br	VPol, repeat after the weekend because 6/16 data didn't match original VPol tests of made on 6/8.
16x16 BLAST	6/18	716.br	VPol repeat.
16x16 BLAST	6/21	718,719.br	Hpol, repeat.
16x16 BLAST	6/21	724.br	Hpol, Set Lo=153 MHz, IF=7MHz

Table C-2. Spectrum Analyzer (CW) Narrowband BLAST Data Files and Descriptions

Data Type	Date	Data File	Description
CW	6/6/02	cw_vpol.txt	VPol, Tx(17), Rx(1-16), P_{TX}=-11.8 dBm
CW	6/11/02	cw_hor.dat	HPol, Tx(17,18,25) Rx(1-16), P_{TX}= -11.8dBm
CW	6/21/02	cw_16x16_hor.dat	Hpol, Tx(1-16),Rx(1-16), P_{TX}= -10.0 dBm

Table C-3. Vector Network Analyzer Antenna Element Coupling Data Files and Descriptions

Data Type	Date	Data File	Description
Ant. Coupling	6/4,5,6	Disks 1-19	VPol, S Parameters, In=A1-A15,Out=A2-A16
Ant. Coupling	6/12/02	Disks 20-39	Hpol, S Parameters, In=A1-A15,Out=A2-A16
Component	3/12/02	Data01-10	Low Pass Filter, Power Divider
AGC Amp	6/29/02	Data01-55	AGC Amp Calibration Data

Table C-4. Anechoic Chamber Antenna Element Calibration Data Files and Descriptions

Data Type	Date	Data Files	Description
E/H Scans	3/1	ITS01,b,c	Antenna #1, E/H co/cross polarization data
E/H Scans	4/6	M-LOC Disk1	TAR Data, E/H, Antennas 1-19
E/H Scans	4/6	M-LOC Disk2	TAR Data, E/H, Antennas 20-35
Mfiles	4/6	Misc.	mfiles for reading and plotting TAR data

APPENDIX D: TRANSMITTER CALIBRATION DATA

Table D-1. Transmitter Power Levels Measured at Coupler and Used for TxCal Data

Transmitter	Power (dBm)
1	-40.44
2	-39.86
3	-40.42
4	-39.65
5	-40.63
6	-40.65
7	-40.87
8	-41.29
9	-40.14
10	-40.42
11	-42.19
12	-41.2
13	-40.53
14	-40.35
15	-41.11
16	-41.01

APPENDIX E: SOFTWARE DESCRIPTION

This section gives an overview of the software developed for the ordering and analysis of the BLAST data.

E.1 CalTx

CalTx is used to read the raw calibration data from 16 transmitter channels and assemble the diagonal elements of the 256-element system response matrix. Calibration data is recorded at 7 power levels for the 16 transmitter channels. These calibration signals are fed into the 16 MUX channels using the same transmit and receive antenna cables used during the BLAST field tests at the NIST OATS. Raw calibration data is stored in four separate data files. Each data file has four channels of data and 7 bursts of data corresponding to the 7 input power levels per channel. Each burst of data has 128 impulses spaced at 3 ms intervals. A total of four data files are needed to store the 16 channels of raw calibration data. Input to CalTx is the first of four sequential raw data file numbers. The program automatically reads the AGC gain phase table and applies these scaling factors to the raw data. Output is $Ctx_{i,j}(w,n)$, $i=j=1,2,3…16,\ n=1,2…7,$ the transmitter system response calibration file at 7 power levels.

E.2 CalRx

CalRx reads raw calibration data using all receiver channels and a single transmitter to calculate the first row of the 256-element system response matrix. The transmitter is connected to the receiver using transmit antenna cable 17 and receive antenna cable 1 connected with an N type barrel. Input power level corresponds to n=2 of the CalTx data. Raw data is stored in 16 separate files, 1 burst per file, 128 impulses per burst at 3 ms intervals. The program also reads the AGC gain phase tables and applies these scaling factors to the raw data. Output is $CRx_{i,j}(w),i=1,j=1,2,3…16,$ the receiver system response matrix.

E.3 CalSys

CalSys reads the transmitter and receiver system response output files from CalRx and CalTx. CalSys then calculates the 256-element system response matrix for the transmitter receiver system. It also calculates *P_cal(16,7),* power calibration factors for all 16 transmitters so that raw data can be scaled to units of *dBm* or *dBm/Hz* if required. Input requirements are: the appropriate HTx.mat and HRx.mat output files from CalRx and CalTx, and the TxPower.txt data file containing the transmitter power levels for the 16 transmitters measured at the end of each transmit antenna cable. The program outputs $CSys_{ij}(w)$, the 256-element system response matrix.

E.4 Praw H_{ij}

Praw H_{ij} processes raw BLAST data files and calculates the 256-element **H** matrix for the BLAST radio channel. The raw data files are arrayed as described in section 7.1. All raw data are scaled by the AGC gain phase and then the 128 IF signals per receiver channel are averaged before down conversion and correlation processing which calculates the channel response *H(w)* for each of the 16 receiving antennas. *H(w)* is then translated to the time domain to separate $h(t)_{ij}$ into its 256 elements after time shifting each of the 16 transmitter signals received at each antenna element to zero phase and zero padding. $h(t)_{ij}$ is then translated back to the frequency domain where the system response is deconvolved using $CSys_{ij}(2)$. Assumptions here are linear phase and constant relative amplitude. By only using frequency 2 (first frequency above 0 at baseband) this avoids deconvolution near the nulls of the system response function and also effects due to local oscillator feed-through at the carrier frequency.

E.5 Praw 1x16

Praw 1x16 processes the raw data for 16 receive antennas when only one transmitter was operational. After arraying the data from the 16 receivers, one transmitter at a time, it follows the same processing algorithm as PrawH_{ij} to calculate the **H** matrix of the 16x16 BLAST channel.